PNNL-27572 Rev. 1

Pacific Northwest
NATIONAL LABORATORY
Proudly Operated by Battelle Since 1965

β-γ Absolute Calibration Rev. 1

January 2019

MW Cooper
JH Ely
JC Hayes
MF Mayer
JI McIntyre
JL Slack

U.S. DEPARTMENT OF ENERGY

Prepared for the U.S. Department of Energy
under Contract DE-AC05-76RL01830

DISCLAIMER

This report was prepared as an account of work sponsored by an agency of the United States Government. Neither the United States Government nor any agency thereof, nor Battelle Memorial Institute, nor any of their employees, makes **any warranty, express or implied, or assumes any legal liability or responsibility for the accuracy, completeness, or usefulness of any information, apparatus, product, or process disclosed, or represents that its use would not infringe privately owned rights**. Reference herein to any specific commercial product, process, or service by trade name, trademark, manufacturer, or otherwise does not necessarily constitute or imply its endorsement, recommendation, or favoring by the United States Government or any agency thereof, or Battelle Memorial Institute. The views and opinions of authors expressed herein do not necessarily state or reflect those of the United States Government or any agency thereof.

PACIFIC NORTHWEST NATIONAL LABORATORY
operated by
BATTELLE
for the
UNITED STATES DEPARTMENT OF ENERGY
under Contract DE-AC05-76RL01830

Printed in the United States of America

Available to DOE and DOE contractors from the
Office of Scientific and Technical Information,
P.O. Box 62, Oak Ridge, TN 37831-0062;
ph: (865) 576-8401
fax: (865) 576-5728
email: reports@adonis.osti.gov

Available to the public from the National Technical Information Service
5301 Shawnee Rd., Alexandria, VA 22312
ph: (800) 553-NTIS (6847)
email: orders@ntis.gov <http://www.ntis.gov/about/form.aspx>
Online ordering: http://www.ntis.gov

This document was printed on recycled paper.
(8/2010)

PNNL-27572 Rev. 1

β-γ Absolute Calibration

MW Cooper
JH Ely
JC Hayes
MF Mayer
JI McIntyre
JL Slack

January 2019

Prepared for
the U.S. Department of Energy
under Contract DE-AC05-76RL01830

Pacific Northwest National Laboratory
Richland, Washington 99352

Contents

Figures

Tables

1.0 Introduction

Identification of nuclear events (Hayes et al. 1999; Ringbom et al. 2003; Le Petit et al. 2008; Prelovskii et al. 2007) rely on accurate measurement of radioxenon releases (Arthur et al. 2001; Auer et al. 2010; Bowyer et al. 1998; Bowyer et al. 2000; Bowyer et al. 2006; Bowyer et al. 2009; Bowyer et al. 2011; Le Petit et al. 2006; McIntyre et al. 2001; Ringbom 2005; Saey 2009; Saey et al. 2013). Measurement of radioxenon relies on accurately knowing the detection efficiency for each isotope.

Four xenon isotopes are of interest: ^{135}Xe, ^{133}Xe, ^{133m}Xe, and ^{131m}Xe. Each isotope has a unique signature; however, there is overlap between each signature. A series of ratio terms, called interference ratios, helps account for the challenges created by the overlap. The ratio and detection efficiency terms are all determined during the initial detector calibration. Additional spectra are needed for a complete calibration: the radon daughter ^{214}Pb/^{214}Bi, the detector background, and the ^{137}Cs quality control (QC) (see Figure 1.1 for spectra not including QC [Reeder et al. 2004]).

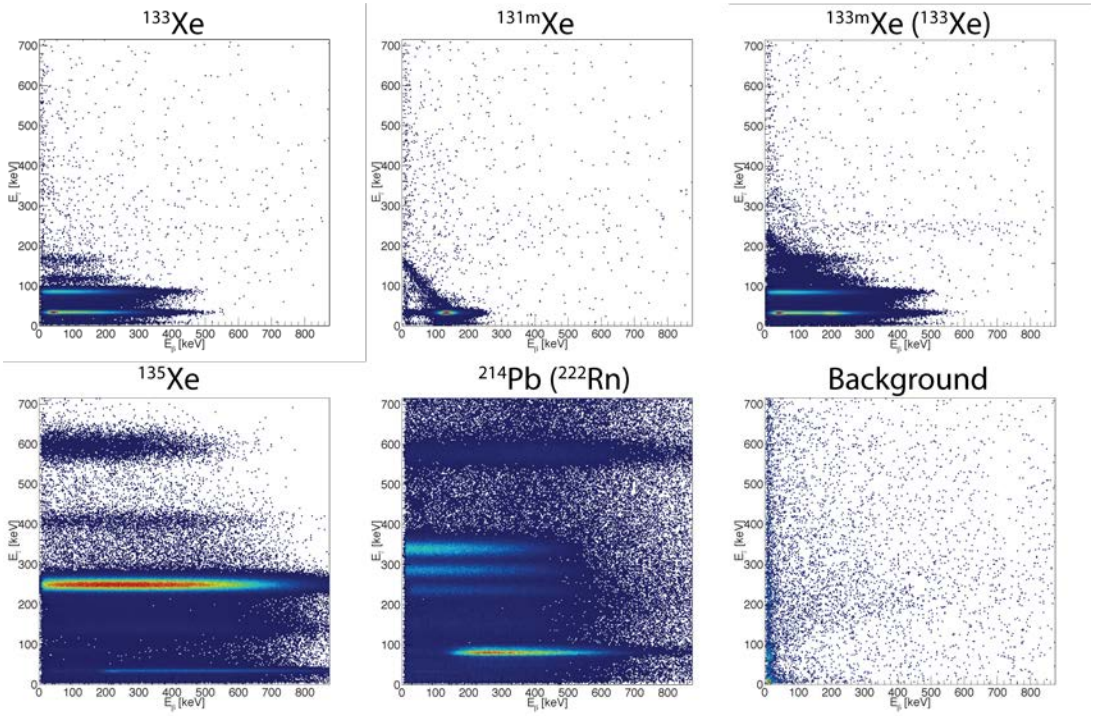

Figure 1.1. Examples of Typical β-γ Calibration Spectra

1.1 β-γ Radioxenon Regions of Interest

The current method used in radioxenon analysis is based on defined regions of interest (ROIs). Each of the five isotopes (^{214}Pb, ^{135}Xe, ^{133}Xe, ^{133m}Xe, and ^{131m}Xe) has one or more defined regions of interest that encompasses the strongest β-γ decay. Based on the defined ROI, interference from other measured isotopes may exist, which are accounted through the previously mentioned interference ratios. The calibration method makes use of the same ROI definitions as used in sample analysis. The definition is based upon the physics of each isotope (see Table 1.1).

Table 1.1. A list of the Regions of Interest used in a seven-region radioxenon analysis. The third column notes the nomenclature used to reference net counts and detection efficiencies associated with a particular ROI.

Region	Isotope of interest	Equation Nomenclature	γ range (keV)	β range (keV)
1	^{222}Rn (352 keV of ^{214}Pb)	R1	313-391	4-672
2	^{135}Xe	R2	220-280	4-830
3	^{133}Xe (80 keV)	R3	63-99	4-346
4	^{133}Xe (30 keV)	R4	15-48	4-392
5	^{131m}Xe	R5	15-48	90-164
6	^{133m}Xe	R6	15-48	165-238
7	^{133}Xe (exclusion)	R7	15-48	87-241
4-7	^{133}Xe	R47	15-48	4-86, 242-392

The ROIs are defined in energy; therefore, the detector energy to channel (and vice versa) needs to be determined. Initial setup of a coarse energy range for the β and γ detectors is performed using a quality assurance/quality control (QA/QC) ^{137}Cs check source, mentioned earlier. However, the actual energy calibration is performed using the xenon calibration spikes. The centroid of each peak is measured and paired with the appropriate energy. Table 1.2 lists typical β and γ energy calibration values. A linear least-squares-fit is then used to convert between energy and channel and aligns the measured data with the defined ROIs.

Table 1.2. A list of energy and corresponding channel for typical peaks measured during the energy calibration of a β-γ detector

β Energy (keV)	Channel	γ Energy (keV)	Channel
129.4	34.6	31.6	11.3
158.4	42.5	81.0	30.1
198.7	59.3	163.9	57.4
		233.2	80.3
		249.8	86.7
		295.2	103.5
		351.9	122.0
		609.4	207.9

A QC measurement should be performed prior to each radioisotope measurement to verify gain stability. The centroid of the 661.7 keV γ peak should be fixed to a specific channel and verified it is in that channel before measurement. The typical placement for the 661.7 keV peak in PNNL developed detector systems is channel 230. The peak is found by fitting a Gaussian to the peak between 550 keV and 700 keV seen in the γ-singles plot in blue in Figure 1.2. The β energy endpoint is determined by

using the Compton scatter line seen in the β-γ spectrum. Fitting a line to the Compton line and extending it to the E_β axis will provide an endpoint energy which the typical placement would be channel 200.

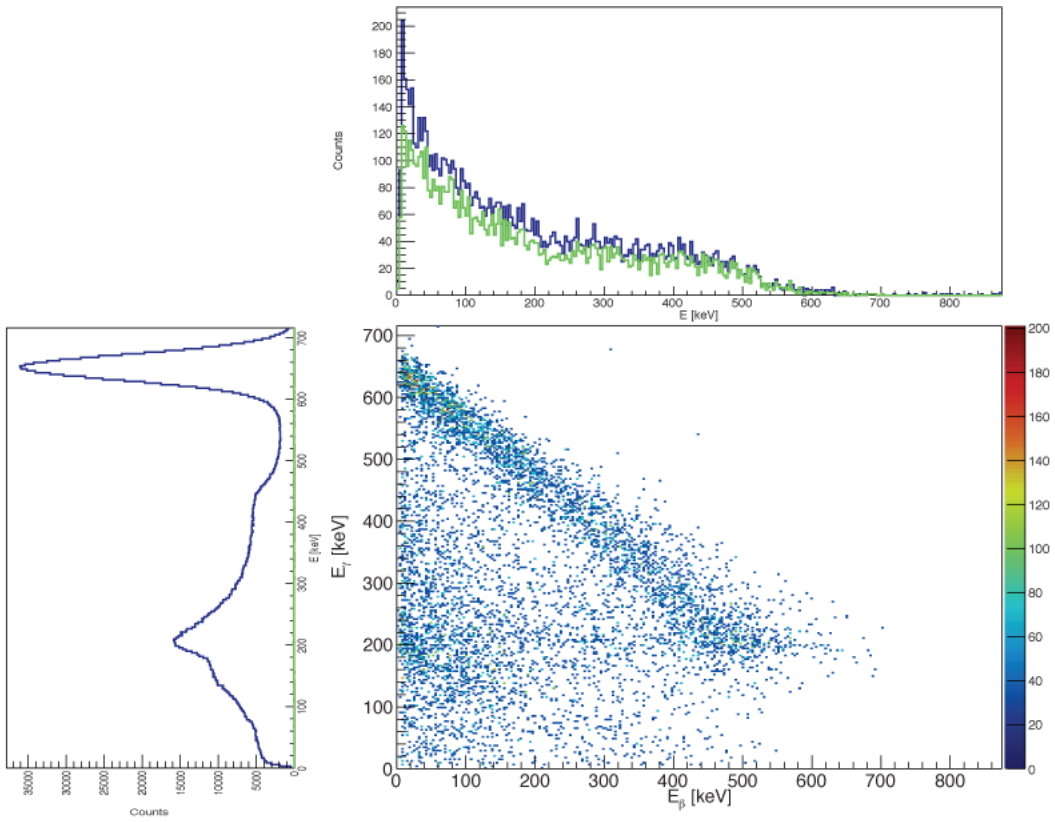

Figure 1.2 Typical ^{137}Cs Calibration Spectra. The top plot is β-singles (blue) and the β projection of the β-γ spectrum (green). The right plot is γ-singles (blue) and the γ projection of the β-γ spectrum (green).

The ROIs determine the number of measured events associated by energy to a given isotope; however, several sources for the counts appear in an ROI. First, there is ambient background radiation that is accounted through subtraction of detector background spectra from the sample of interest. Second, there may be a residual sample (memory effect) that needs to be accounted for through a gas background file. The gas background file measures the residual radioxenon present from previous samples. Finally, there is potential interference between isotopes that are present in the sample. In a calibration all of these terms may be present. However, if the calibration gases are introduced to minimize the memory effect, then only the detector background needs to be accounted and the interference terms will be measured for each calibration sample. The interference terms are simply a ratio of the net counts for each ratio. In the case of ^{214}Pb, six ratios will be calculated (see Table 1.3).

Table 1.3. Interference ratio terms determined during the calibration process

	R2	R3	R4	R5	R6	R47
^{214}Pb	$\frac{C_{Net_{ROI2}}}{C_{Net_{ROI1}}}$	$\frac{C_{Net_{ROI3}}}{C_{Net_{ROI1}}}$	$\frac{C_{Net_{ROI4}}}{C_{Net_{ROI1}}}$	$\frac{C_{Net_{ROI5}}}{C_{Net_{ROI1}}}$	$\frac{C_{Net_{ROI6}}}{C_{Net_{ROI1}}}$	$\frac{C_{Net_{ROI47}}}{C_{Net_{ROI1}}}$
^{135}Xe		$\frac{C_{Net_{ROI3}}}{C_{Net_{ROI2}}}$	$\frac{C_{Net_{ROI4}}}{C_{Net_{ROI2}}}$	$\frac{C_{Net_{ROI5}}}{C_{Net_{ROI2}}}$	$\frac{C_{Net_{ROI6}}}{C_{Net_{ROI2}}}$	$\frac{C_{Net_{ROI47}}}{C_{Net_{ROI2}}}$
^{133}Xe				$\frac{C_{Net_{ROI5}}}{C_{Net_{ROI3}}}$	$\frac{C_{Net_{ROI6}}}{C_{Net_{ROI3}}}$	

The interference ratios are calculated with the assumption that the samples are isotopically pure, but additional data analysis may be performed to account for impurities or contaminates present in the samples. Additionally, every measurement has a background component that relates to the environmental radiation (i.e., the thorium content of concrete flooring will influence the detector background based on distance). The background is assumed to be constant in that it will be composed of long-lived isotopes that appear constant for the relatively short duration of the calibration measurement. Therefore, the net counts are the gross counts with the background subtracted out:

$$\boldsymbol{Counts_{Net} = Counts_{Gross} - Counts_{Background}}$$

$$\boldsymbol{-Counts_{Interf}erence - Counts_{Memory}} \quad \text{Eq. 1}$$

However, $\boldsymbol{Counts_{Interference}}$ and $\boldsymbol{Counts_{Memory}}$ do not need to be accounted for during a calibration since they are not present; a radioxenon calibration spike is isotopically pure (except for ^{133m}Xe) and spikes introduced after each previous spike has decayed away. Therefore, the net counts has a simpler equation:

$$\boldsymbol{Counts_{Net} = Counts_{Gross} - Counts_{Background}} \quad \text{Eq. 2}$$

The ROIs are also used to calculate the detection efficiency. In the remaining sections of this report, the counts used in the equations represent background-subtracted counts in the defined ROI range. However, there is a special situation for cases where β singles counts are used. Since the β single counts will contain events that have β, conversion electrons, and Auger electrons, the energy range needs to be extended to higher energy than the β endpoint would suggest. The typical β single-energy range used in the calculation will cover the full β continuum, but care must be taken to not include any signal noise within the range. If noise is present, the range may need to be reduced to remove the extra counts from the calibration analysis.

1.2 Calibration Methods

Three typical calibration methods are employed in characterizing a nuclear detector. The first and easiest method is to use a radioactive source standard, or National Institute of Science and Technology

(NIST) standard. In this method, the activity of a source is accurately measured using a calibrated detector standard. The measured source activity (often considered a known source) is then used to determine what the detection efficiencies are for the nuclear detector of interest. This method is only as accurate as the calibration of the well-known detector. Another limitation is the selection of isotopes that have γ-rays at or near the energies expected from a sample. For radioxenon measurements this will be approximately 30, 80, and 250 keV. When using a γ source standard, it is often necessary to interpolate the efficiency results to the energies of interest, which adds to the overall measurement uncertainty. An alternative calibration source is radioactive xenon gas standards, which have known activities and should have a gas composition matching the composition of an expected sample.

Another more accurate calibration method is to calibrate with a radioactive sample that has been measured using a well-characterized nuclear detector. This method will remove the necessity of interpolating between energies since the calibration source can be the same material expected for sample measurements. In the case of radioxenon, this would be one of the four xenon isotopes of interest (^{135}Xe, ^{133m}Xe, ^{133}Xe, and ^{131m}Xe). However, this method is still reliant on how well the efficiency calibration is known for the well-characterized nuclear detector. Furthermore, understanding the uncertainties in a gas sample transfer is extremely challenging and is an additional calibration uncertainty.

Because of the difficulties in the previous methods, a third method has been chosen for β-γ nuclear detector calibration at Pacific Northwest National Laboratory (Bowyer et al. 1999; Carman et al. 2005; Cooper et al. 2005; Cooper et al. 2007a; Cooper et al. 2007b; Hennig et al. 2006a, Hennig et al. 2006b; Hennig et al. 2007; McIntyre et al. 2001; McIntyre et al. 2007; Ringbom et al. 2003). The third method exploits the β-γ coincident measurement to make an absolute activity measurement (Cooper et al. 2013a; Cooper et al. 2013b; Ely et al. 2010; Knoll 2010; McIntyre et al. 2012; NCRP 1985) and, consequently, an efficiency calibration. The absolute efficiency calibration method uses the four-radioxenon isotopes (^{135}Xe, ^{133m}Xe, ^{133}Xe, and ^{131m}Xe), radon (^{214}Pb), and detector background files as the calibration standard (see Figure 1.1 for examples). The method is not reliant upon a known activity sample because it inherently determines the absolute activity, but does need isotopically pure samples to obtain an accurate calibration.

1.3 β-γ Calibration Methodology

The calibration technique discussed in this document can be used for any coincident detection system; however, for β-γ systems that have near 4π solid angle coverage, the components that need to be accounted for will make the method extremely complex. For the β–γ calibration discussed in this paper, several simplifications can be used (Knoll 2010). For instance, the detector geometry allows for nearly 4π solid angle coverage for β-decay, meaning the sample is surrounded by the β-detector. This allows angular correlations among radiation types to be ignored (NCRP 1985). In addition, the radioxenon samples are produced in nearly radioisotopically pure form, and no complicating radioactive interference terms exist (Gohla et al. 2016; Haas et al. 2009; Houghton et al. 2016; McGrath et al. 2013; McIntyre et al. 2008; Watrous et al. 2015). This specific method leverages the β-γ coincidence detection to determine the total number of decays (or absolute activity) by comparison among the numbers of β-single, γ-single, and β-γ coincidence detected decays. The total decays (ΔN) can be written in three different forms, one for each type of decay: β-γ, γ and β.

$$\Delta N = \frac{C_{\beta\gamma}}{BR_{\beta\gamma}\varepsilon_{\beta\gamma}} = \frac{C_{\beta\gamma}}{BR_{\gamma}\varepsilon_{\beta\gamma}} \quad \text{Eq. 3}$$

$$\Delta N = \frac{C_{\gamma}}{BR_{\gamma}\varepsilon_{\gamma}} \quad \text{Eq. 4}$$

$$\Delta N = \frac{C_{\beta}}{1-(1-\varepsilon_{\beta})\left(1-\varepsilon_{CE_i}BR_{CE_i}\right)} \quad \text{Eq. 5}$$

Where *BR* is the known branching ratio, ε is the detection efficiency, $C_{\beta\gamma}$ is the number of decay events observed in the β-γ detector, and the subscript symbols γ, and β and *CE* (conversion electron) are radiation types.

By solving Eq. 3 with respects to Eq. 4, it is possible to determine the absolute effective β efficiency (ε_{β}) for the particular ROI. However, the most complex and difficult efficiency to determine is the γ efficiency because of the multiple decay paths. Each decay path offers another opportunity to detect a β or CE, which will increase the probability that any given nuclear decay is observed. These additional decay paths are taken into account by determining the probability that any one nuclear decay is detected. In the calculations that appear later in this document, a decay path may have an effective efficiency associated with it, which will be used to determine the overall effective isotopic detection efficiency. The effective efficiency is often the combined detection efficiency for the β decay as well as a CE or Auger electron (AE). To discriminate between the effective detection efficiencies for the different decay paths a nomenclature for the efficiency terms will be implemented. The efficiency terms may have two components as a subscript; the first term will identify the primary decay (either β, CE, or AE), while the second term will have γ- or X-ray energy associated with the β/CE/AE coincident decay.

An example of the complexity of the calculation is ^{133}Xe. As can be seen in Figure 1.2, the primary signatures for ^{133}Xe are the 80.997-keV γ-ray in coincidence with a β, and the 31.606-keV X-ray in coincidence with a 45-keV CE. However, two other decay paths can occur in anti-coincidence with the primary. The additional decay paths result in several terms that need to be included in the calibration calculation.

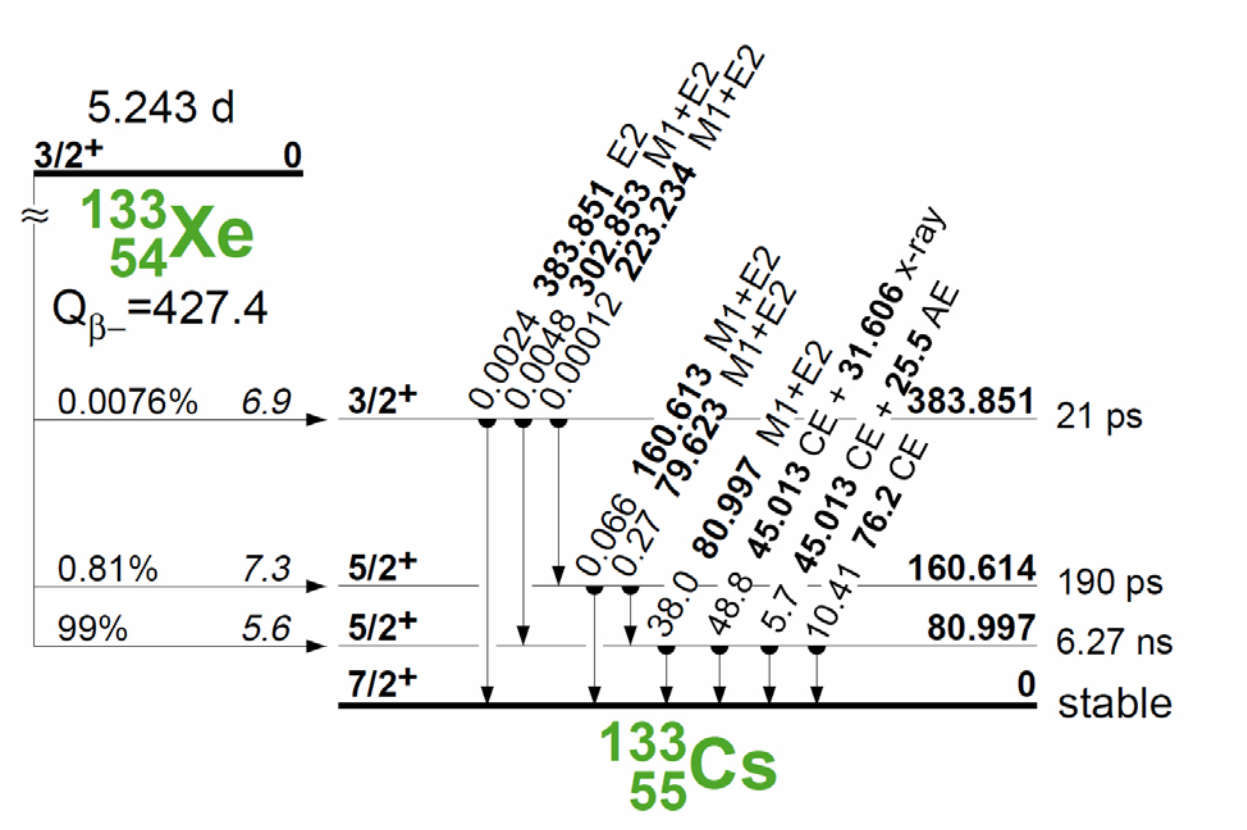

Figure 1.3. Decay Scheme from ^{133}Xe to ^{133}Cs with Additional Internal Conversion Decay Process Included (Cooper et al. 2013a)

1.4 Radioxenon Samples

One other critical component to the calibration of radioxenon β-γ systems is the availability of isotopically pure xenon. Four radioxenon isotopes are of interest as nuclear explosion signatures and calibration sources. Until recently, only two of the four have been available. Both ^{133}Xe and ^{131m}Xe have been available through standard medical isotope facilities. However, Idaho National Laboratory and University of Texas have built the capability to supply ^{135}Xe (Figure 1.4a) and ^{133m}Xe (Figure 1.4b) in addition to the other two xenon isotopes.

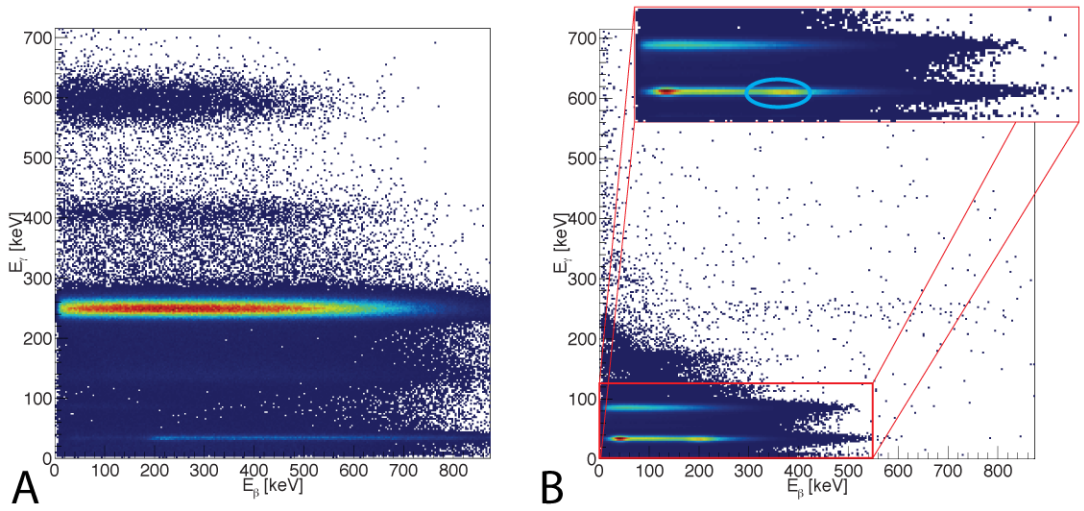

Figure 1.4. A: β-γ Coincidence Plot of the ^{135}Xe Calibration Sample Data. B: β-γ Coincidence Plot of the ^{133m}Xe Calibration Sample Data with ^{133}Xe and a Small Contaminate of ^{135}Xe. The region in Figure B circled in blue within the expanded ^{133m}Xe region is the ^{133m}Xe β-γ coincidence peak, and the other horizontal peak is ^{133}Xe.

The availability of all four xenon isotopes allows the absolute calibration of β-γ systems for all four isotopes. However, several constraints to the calibration exist. First are time constraints for the calibration of the systems. Each radioxenon isotope has a different half-life, so it is important to calibrate the β-γ systems using the correct radioxenon sample order. The order progresses from the shortest half-life (^{135}Xe) isotope to the longest-lived (^{131m}Xe), which allows for the fastest calibration. In addition, because of the memory effect in the β cell, adequate time needs to be given for each radioxenon isotope to decay away prior to the introduction of a new radioxenon isotope. The process will take approximately one month to complete, based upon the timeline in Table 1.4, and includes measuring the ambient background.

Table 1.4. Calibration Process Timeline. Times are selected to work within normal business hours and sample shipment restrictions (assumed process begins on a Friday at 8:00 a.m.).

	Process	Time (days)
^{137}Cs	Setup, energy calibrate, gain matching	0.5
Detector Background	Background collection	~3.5
^{135}Xe	Count	0.5
	Pump and flush (delay for decay)	2
	Gas background	0.5
^{133}Xe	Count	0.5
	Pump and flush (delay for decay)	6
	Gas background	0.5
$^{133m/133}Xe$	Count	0.5
	Pump and flush (delay for decay)	6
	Gas background	0.5
^{131m}Xe	Count	0.5
	Pump and flush (delay for decay)	12
	Gas background	0.5
Radon	Count	0.5
	Pump and flush (delay for decay)	2
Total time		36.5 days

A second constraint to the calibration is the importance of a very precise low-uncertainty measurement. Although the calibration method is usable for standard sample measurements because it determines the absolute activity present, standard samples typically have very low counting statistics and result in conditions that will bias the system. Consequently, it is desirable to determine the β-γ detection efficiency to very high accuracy in a calibration setting and avoid additional uncertainty terms. This high-accuracy detection efficiency requires high counting statistics, and therefore high-activity samples. In general, the uncertainty inherent in a measurement due to the counting statistics is the square root of the number of counts in the ROI. Therefore, to obtain a 1% statistical uncertainty, more than 10000 net counts in the ROI are necessary because uncertainties propagate for each term subtracted (including background and any other interference terms).

In all cases one must account for background radiation (see Eq. 6). This means that a shorter calibration sample count time is desirable to reduce the impact of the background term, which is estimated as being a constant activity source. Furthermore, the longer the time the calibration samples reside in the plastic scintillating β cell, the more radioxenon uptake there is (also known as memory effect). A typical memory effect for plastic β cells is 3% to 5%, but the actual percentage is dependent on residence times. These effects drive the sample activity and time limits at the point of introduction into the system.

$$\Delta C = C_{sample} - C_{background} * \frac{Livetime_{sample}}{Livetime_{background}} \qquad \text{Eq. 6}$$

Finally, small amounts of contaminants are present in the samples. These contaminants are a very small fraction of the total activity, but begin to be observable in the data after several half-lives of the sample isotope of interest; therefore, the samples need to be measured in the β-γ detector relatively quickly based on the isotope half-life. For instance, ^{135}Xe has a 9.14-hour half-life and has a small ^{133}Xe contaminant with a 5.243-day half-life. This means that after two days the ^{133}Xe will begin to influence the ^{135}Xe calibration results. The presence of contaminants primarily affects ^{135}Xe and ^{133m}Xe because of their shorter half-lives. Pacific Northwest National Laboratory recommends measurement of ^{135}Xe within one day of irradiation to reduce this effect.

The next four sections of this document systematically provide the calculations to determine the detection efficiencies for each isotope and region of interest. In this document the X-ray detected for each of the four isotopes will be referred to as 32-keV even though it is a sum of several X-rays and the branching ratio weighted mean energy can vary from 32-keV by ± 2-keV. γ-ray energy will be referenced as 81 or 250-keV when in fact they may be slightly higher or lower as seen in Figures 2.1, 3.1, 4.1, and 5.1.

2.0 Detection Efficiencies for ^{133}Xe

The most complex isotope, in terms of decay structure, is ^{133}Xe. It goes through a β decay followed by a prompt (6.27 ns) γ-ray decay (Figure 2.1). However, additional decay mechanisms come into play (Cooper et al. 2013a). The decay mechanisms are β/γ-ray, $\beta/$X-ray/CE, $\beta/$CE/AE, and $\beta/$CE. As of this report's publication, the quad detector is unable to differentiate CE from β and X-ray from γ-ray, so there are three calculation methods (β, γ, and β-γ) for determining the total decays (ΔN). Spectra showing the three channels of decay are shown in Figure 2.2. The equations in this section step through the process used to determine the detection efficiencies for the β-γ nuclear detector. Five basic equations represent the β-singles (Eq. 133-1), γ-singles (Eq. 133-2 and Eq. 133-3), and β-γ (Eq. 133-4 and Eq. 133-5) coincidence for the two primary decay signatures: 80-keV γ-ray and 30-keV X-ray.

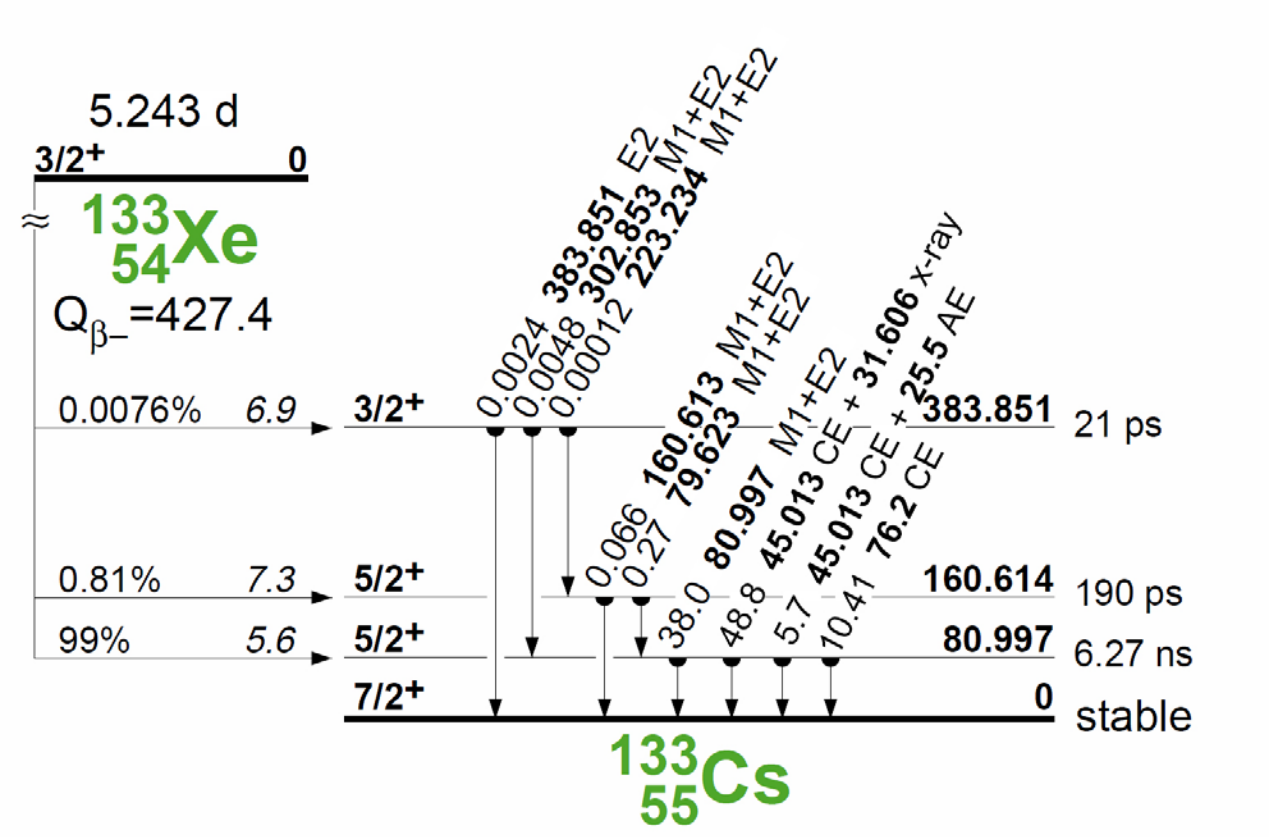

Figure 2.1. Decay scheme from ^{133}Xe to ^{133}Cs with additional internal conversion decay process included (Cooper et al. 2013a)

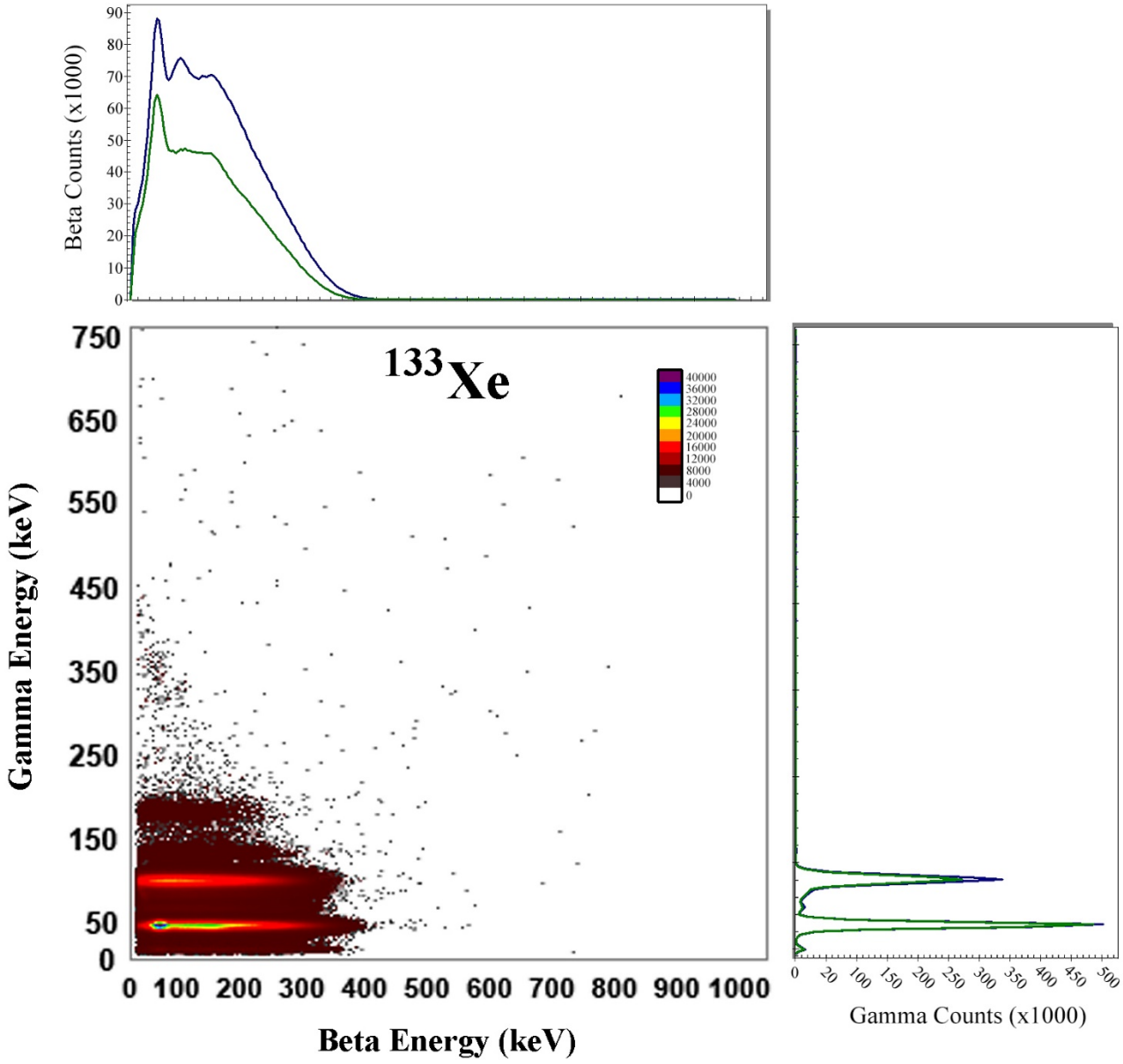

Figure 2.2. Typical ^{133}Xe Calibration Spectra. The top plot is β-singles (blue) and the β projection of the β-γ spectrum (green). The right plot is γ-singles (blue) and the γ projection of the β-γ spectrum (green).

$$\boldsymbol{\Delta N = \frac{C_{\beta}}{BR_{\gamma 81}\cdot\varepsilon_{\beta R3}+\begin{bmatrix} BR_{CE76}\cdot\left[1-\left(1-\varepsilon_{\beta}\right)\cdot\left(1-\varepsilon_{CE76}\right)\right] \\ +BR_{\gamma 32}\cdot\left[1-\left(1-\varepsilon_{\beta}\right)\cdot\left(1-\varepsilon_{CE45}\right)\right] \\ +BR_{AE26}\cdot\left[1-\left(1-\varepsilon_{\beta}\right)\cdot\left(1-\varepsilon_{CE45}\right)\cdot\left(1-\varepsilon_{AE26}\right)\right]\end{bmatrix}}}$$ Eq. 133- 1

Where, $BR_{CE45} \cong BR_{\gamma 32} + BR_{AE26}$ due to the 31.6-keV X-ray and 25.5-keV AE being the primary decay methods in coincidence with the 45-keV CE.

$$\boldsymbol{\Delta N = \frac{C_{\gamma R3}}{BR_{\gamma 81}\cdot\varepsilon_{\gamma R3}}}$$ Eq. 133- 2

$$\boldsymbol{\Delta N = \frac{C_{\gamma R4}}{BR_{\gamma 32}\cdot\varepsilon_{\gamma R4}}}$$ Eq. 133- 3

$$\boldsymbol{\Delta N = \frac{C_{\beta\gamma R3}}{BR_{\beta\gamma 81}\cdot\varepsilon_{\beta\gamma R3}} = \frac{C_{\beta\gamma R3}}{BR_{\gamma 81}\cdot\varepsilon_{\beta\gamma R3}}}$$ Eq. 133- 4

$$\boldsymbol{\Delta N = \frac{C_{\beta\gamma R4}}{BR_{\gamma 32}\cdot\varepsilon_{\beta\gamma R4}}}$$ Eq. 133- 5

Where $\boldsymbol{\varepsilon_{\beta\gamma R4} = \varepsilon_{\beta R4}\varepsilon_{\gamma R4}}$, and furthermore $\boldsymbol{\varepsilon_{\beta R4} = \left[1-\left(1-\varepsilon_{\beta R3}\right)\cdot\left(1-\varepsilon_{CE45}\right)\right]}$

$BR_{\beta\gamma 81} \cong BR_{\gamma 81} = 0.380 \pm 0.007$
$BR_{\beta} = 0.999 \pm 0.014$
$BR_{CE76} = 0.1041 \pm 0.0016$
$BR_{CE45} = 0.56 \pm 0.01$
$BR_{AE26} = 0.057 \pm 0.002$
$BR_{\gamma 32} = 0.488 \pm 0.015$

The first step in determining the detection efficiency is to pick the simplest decay path. In the case of ^{133}Xe, the 80-keV γ-ray in coincidence with a β is the simplest path (contains the least number of radiation types and energies). Using Eq. 133-2 and 133-4, one forms Eq. 133-6.

$$\boldsymbol{\Delta N = \frac{C_{\beta\gamma R3}}{BR_{\gamma 81}\cdot\varepsilon_{\beta\gamma R3}} = \frac{C_{\gamma R3}}{BR_{\gamma 81}\cdot\varepsilon_{\gamma R3}}}$$ Eq. 133- 6

The β efficiency is calculated by comparing the observed 80-keV γ-ray decays with the 80-keV γ-ray decays in coincidence with the β decay.

$$\boldsymbol{C_{\beta\gamma R3}\cdot BR_{\gamma 81}\cdot\varepsilon_{\gamma R3} = C_{\gamma R3}\cdot BR_{\gamma 81}\cdot\varepsilon_{\beta\gamma R3}}$$ Eq. 133- 7

Since $\varepsilon_{\beta\gamma} = \varepsilon_{\beta}\cdot\varepsilon_{\gamma}$, Eq. 133-7 may be rewritten as Eq. 133-8

$$\boldsymbol{C_{\beta\gamma R3}\cdot \cancel{BR_{\gamma 81}}\cdot \cancel{\varepsilon_{\gamma R3}} = C_{\gamma R3}\cdot \cancel{BR_{\gamma 81}}\cdot\varepsilon_{\beta}\cdot \cancel{\varepsilon_{\gamma R3}}}$$ Eq. 133- 8

After canceling terms and solving for the β efficiency, Eq.133-8 can be simplified to Eq. 133-9.

$$\boldsymbol{\varepsilon_{\beta R3}} = \frac{C_{\beta\gamma R3}}{C_{\gamma R3}} \qquad \text{Eq. 133- 9}$$

Once the β efficiency has been calculated, the next step is to determine the more complicated decay efficiencies. The 30-keV X-ray is in coincidence with a β and CE. Once again, a comparison between γ-singles and β-γ observed decays is used to determine the detection efficiency for a 45-keV CE. Eq. 133-10 can be written using Eq. 133-3 and Eq. 133-5.

$$\boldsymbol{\Delta N} = \frac{C_{\beta\gamma R4}}{BR_{\gamma 32}\cdot\varepsilon_{\gamma R4}\cdot\varepsilon_{\beta\gamma R4}} = \frac{C_{\gamma R4}}{BR_{\gamma 32}\cdot\varepsilon_{\gamma R4}} \qquad \text{Eq. 133- 10}$$

Eq. 133-11 shows the cancellation of terms from Eq. 133-10 and the substitution of variable $\boldsymbol{\varepsilon_{\beta\gamma R4}}$.

$$\frac{C_{\beta\gamma R4}}{\cancel{BR_{\gamma 32}\cdot\varepsilon_{\gamma R4}}\cdot\left[1-\left(1-\varepsilon_{\beta R3}\right)\cdot\left(1-\varepsilon_{CE45}\right)\right]} = \frac{C_{\gamma R4}}{\cancel{BR_{\gamma 32}\cdot\varepsilon_{\gamma R4}}} \qquad \text{Eq. 133- 11}$$

Eq. 133-12 through Eq. 133-14 show the regrouping of terms from Eq. 133-11, and arrive at the solution for the 45-keV CE efficiency shown in Eq. 133-15.

$$\frac{C_{\beta\gamma R4}}{C_{\gamma R4}} = \mathbf{1} - \left(\mathbf{1} - \boldsymbol{\varepsilon_{\beta R3}}\right)\cdot\left(\mathbf{1} - \boldsymbol{\varepsilon_{CE45}}\right) \qquad \text{Eq. 133- 12}$$

$$1 - \frac{C_{\beta\gamma R4}}{C_{\gamma R4}} = \left(\mathbf{1} - \boldsymbol{\varepsilon_{\beta R3}}\right)\cdot\left(\mathbf{1} - \boldsymbol{\varepsilon_{CE45}}\right) \qquad \text{Eq. 133- 13}$$

$$\mathbf{1} - \boldsymbol{\varepsilon_{CE45}} = \frac{\left(1-\frac{C_{\beta\gamma R4}}{C_{\gamma R4}}\right)}{\left(1-\varepsilon_{\beta R3}\right)} \qquad \text{Eq. 133- 14}$$

$$\boldsymbol{\varepsilon_{CE45}} = 1 - \frac{\left(1-\frac{C_{\beta\gamma R4}}{C_{\gamma R4}}\right)}{\left(1-\varepsilon_{\beta R3}\right)} \qquad \text{Eq. 133- 15}$$

The next step is to solve Eq. 133-1 and 133-2 in terms of the β-γ detection efficiency for the 81-keV region of interest (ROI-3). However, by assuming

$$\boldsymbol{\varepsilon_{CE45} = \varepsilon_{CE76} = \varepsilon_{AE26}}, \qquad \text{Eq. 133- 16}$$

Eq. 133-1 becomes

$$\boldsymbol{\Delta N} = \frac{C_{\beta\gamma R3}}{BR_{\gamma 81}\cdot\varepsilon_{\beta\gamma R3}} = \frac{C_{\beta}}{BR_{\gamma 81}\cdot\varepsilon_{\beta R3} + \begin{bmatrix} BR_{CE76}\cdot\left[1-\left(1-\varepsilon_{\beta R3}\right)\cdot\left(1-\varepsilon_{CE76}\right)\right] \\ +BR_{\gamma 32}\cdot\left[1-\left(1-\varepsilon_{\beta R3}\right)\cdot\left(1-\varepsilon_{CE45}\right)\right] \\ +BR_{AE26}\cdot\left[1-\left(1-\varepsilon_{\beta R3}\right)\cdot\left(1-\varepsilon_{CE45}\right)\cdot\left(1-\varepsilon_{AE26}\right)\right] \end{bmatrix}} \qquad \text{Eq. 133- 17}$$

Setting Eq. 133-15 equal to Eq. 133-16 results in Eq. 133-17. After combining terms in Eq. 133-17 one arrives at Eq. 133-18.

$$C_{\beta} \cdot BR_{\gamma 81} \cdot \varepsilon_{\beta\gamma R3} = C_{\beta\gamma R3} \cdot \left[BR_{\gamma 81} \cdot \varepsilon_{\beta R3} + \begin{bmatrix} BR_{CE76} \cdot \left[1 - \left(1 - \varepsilon_{\beta R3}\right) \cdot \left(1 - \varepsilon_{CE76}\right)\right] \\ +BR_{\gamma 32} \cdot \left[1 - \left(1 - \varepsilon_{\beta R3}\right) \cdot \left(1 - \varepsilon_{CE45}\right)\right] \\ +BR_{AE26} \cdot \left[1 - \left(1 - \varepsilon_{\beta R3}\right) \cdot \left(1 - \varepsilon_{CE45}\right) \cdot \left(1 - \varepsilon_{AE26}\right)\right] \end{bmatrix} \right] \quad \text{Eq. 133- 18}$$

Eq. 133-19 is determined by solving Eq. 133-18 in terms of the 81-keV β-γ efficiency.

$$\varepsilon_{\beta\gamma R3} = \frac{C_{\beta\gamma R3} \cdot \left[BR_{\gamma 81} \cdot \varepsilon_{\beta R3} + \begin{bmatrix} BR_{CE76} \cdot \left[1 - \left(1 - \varepsilon_{\beta R3}\right) \cdot \left(1 - \varepsilon_{CE76}\right)\right] \\ +BR_{\gamma 32} \cdot \left[1 - \left(1 - \varepsilon_{\beta R3}\right) \cdot \left(1 - \varepsilon_{CE45}\right)\right] \\ +BR_{AE26} \cdot \left[1 - \left(1 - \varepsilon_{\beta R3}\right) \cdot \left(1 - \varepsilon_{CE45}\right) \cdot \left(1 - \varepsilon_{AE26}\right)\right] \end{bmatrix} \right]}{BR_{\gamma 81} \cdot C_{\beta}} \quad \text{Eq. 133- 19}$$

Once the β-γ detection efficiency has been determined for ROI-3, it can be used to calculate the total number of ^{133}Xe decays, ΔN, which is then used to determine the remaining detection efficiency terms for ^{133}Xe. The remaining equations march through the efficiency calculations, keeping the variables in terms of basic quantities (i.e., counts in a given ROI). The next decay involves the X-rays that have an average energy of 32-keV X-ray in coincidence with a 45-keV CE and the β. Using the result of Eq. 133-19 and the ratio between Eq. 133-4 and Eq. 133-5, one arrives at Eq. 133-20 and Eq. 133-21.

$$\Delta N = \frac{C_{\beta\gamma R3}}{BR_{\gamma 81} \cdot \varepsilon_{\beta\gamma R3}} = \frac{C_{\beta\gamma R4}}{BR_{\gamma 32} \cdot \varepsilon_{\beta\gamma R4}} \quad \text{Eq. 133- 20}$$

$$\varepsilon_{\beta\gamma R4} = \frac{C_{\beta\gamma R4} \cdot BR_{\gamma 81} \cdot \varepsilon_{\beta\gamma R3}}{C_{\beta\gamma R3} \cdot BR_{\gamma 32}} \quad \text{Eq. 133- 21}$$

$$\Delta N = \frac{C_{\beta\gamma R3}}{BR_{\gamma 81} \varepsilon_{\beta\gamma R3}} = \frac{C_{\gamma R4}}{BR_{\gamma 32} \varepsilon_{\gamma R4}} \quad \text{Eq. 133- 22}$$

$$\varepsilon_{\gamma R4} = \frac{C_{\gamma R4} \cdot BR_{\gamma 81} \cdot \varepsilon_{\beta\gamma R3}}{C_{\beta\gamma R3} \cdot BR_{\gamma 32}} \quad \text{Eq. 133- 23}$$

$$\varepsilon_{\beta R3} = \frac{\varepsilon_{\beta\gamma R3}}{\varepsilon_{\gamma R3}} = \frac{C_{\beta\gamma R3}}{C_{\gamma R3}} \quad \text{Eq. 133- 24}$$

$$\varepsilon_{\beta R4} = \frac{\varepsilon_{\beta\gamma R4}}{\varepsilon_{\gamma R4}} = \frac{C_{\beta\gamma R3}}{C_{\gamma R3}} \quad \text{Eq. 133- 25}$$

Note that ROI-7 is a special case in that the defined energy boundaries make an excluded region, which is used to select observed decays that will not be affected by the presence of metastable isotopes (i.e., excludes ROI-5 and ROI-6). The efficiencies and interference ratios associated with ROI-7 are actually ROI-7 subtracted from ROI-4. Furthermore, the gamma efficiency for the region of interest (ROI-47) defined as ROI-4 – ROI-7 uses $\varepsilon_{\gamma R4}$ for the gamma efficiency, but has an independently determined beta efficiency.

$$\Delta N = \frac{C_{\gamma R4}}{BR_{\gamma 32} \cdot \varepsilon_{\gamma R4}} = \frac{C_{\beta\gamma R47}}{BR_{\gamma 32} \cdot \varepsilon_{\beta_{R47}} \cdot \varepsilon_{\gamma R4}} \quad \text{Eq. 133- 26}$$

$$\boldsymbol{\varepsilon_{\beta R47}} = \frac{\boldsymbol{C_{\beta\gamma R47}}}{\boldsymbol{C_{\gamma R4}}}$$ Eq. 133- 27

3.0 Detection Efficiencies for ^{131m}Xe

^{131m}Xe is the cornerstone for β-γ calibration because of its relatively simple signature, Gaussian distribution in both γ and β. Although the signature is easily fit with Gaussian peaks, the β single events do hide some underlying complexity. ^{131m}Xe decays through CE and X-ray/CE (Figures 3.1 and 3.2).

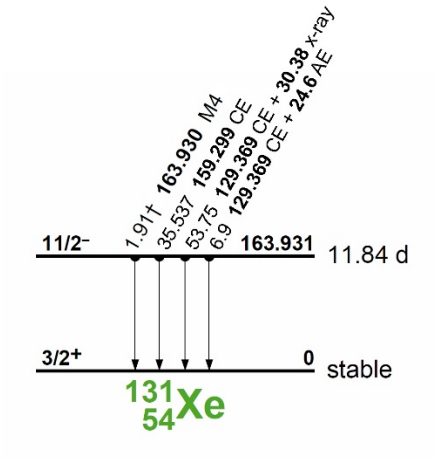

Figure 3.1. Decay scheme from ^{131m}Xe to ^{131}Xe with additional internal conversion decay processes included

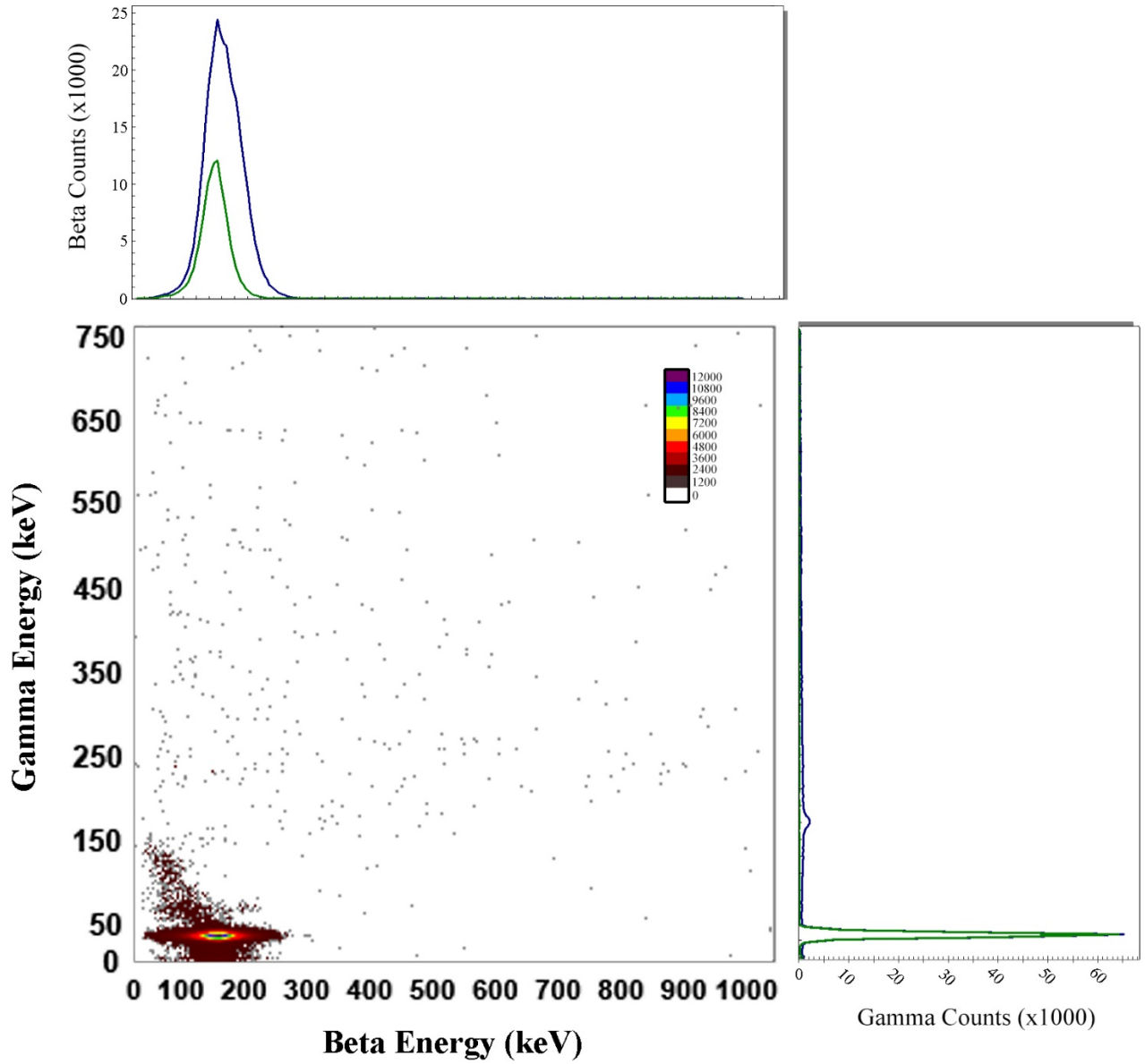

Figure 3.2. Typical ^{131m}Xe calibration spectra. The top plot is of β-singles (blue) and the β projection of the β-γ spectrum (green). The right plot is of γ-singles (blue) and the γ projection of the β-γ spectrum (green).

Noting that $\varepsilon_{\beta\gamma} = \varepsilon_{\beta} \cdot \varepsilon_{\gamma}$.

$$\boldsymbol{\Delta N} = \frac{\boldsymbol{C_{\beta\gamma R5}}}{\boldsymbol{BR_{\beta\gamma R5} \cdot \varepsilon_{\beta\gamma R5}}} = \frac{\boldsymbol{C_{\beta\gamma R5}}}{\boldsymbol{BR_{\gamma 30} \cdot \varepsilon_{\gamma 30} \cdot \varepsilon_{CE129}}} \qquad \text{Eq. 131m- 1}$$

$$\boldsymbol{\Delta N} = \frac{\boldsymbol{C_{\gamma R5}}}{\boldsymbol{BR_{\gamma 30} \cdot \varepsilon_{\gamma R5}}} \qquad \text{Eq. 131m- 2}$$

$$\boldsymbol{\Delta N} = \frac{\boldsymbol{C_{\beta R5}}}{\boldsymbol{BR_{CE160} \cdot \varepsilon_{CE160} + BR_{\gamma 30} \cdot \varepsilon_{CE129} + BR_{AE25} \cdot [1 - (1 - \varepsilon_{CE129}) \cdot (1 - \varepsilon_{AE25})]}} \qquad \text{Eq. 131m- 3}$$

However, since 129-keV and 160-keV CE are nearly the same energy, the efficiencies should be nearly the same, for this reason $\boldsymbol{\varepsilon_{CE129} = \varepsilon_{CE160}}$.

The branching ratios for ^{131m}Xe are given as follows:

$$BR_{\beta\gamma} = BR_{\gamma 30} = 53.8\%$$
$$BR_{CE129} = 61.6\%$$
$$BR_{CE160} = 35.5\%$$
$$BR_{AE25} = 6.9\%$$
$$BR_{Total} = BR_{CE129} + BR_{CE160} = 97.1\%$$

Therefore, Eq. 131m-3 can be simplified to only contain efficiency terms for the 129-keV CE and the 24.6-keV AE (see Eq. 131m-4).

$$\boldsymbol{\Delta N = \frac{C_\beta}{(BR_{CE160}+BR_{\gamma 30})\cdot\varepsilon_{CE129}+BR_{AE25}\cdot[1-(1-\varepsilon_{CE129})\cdot(1-\varepsilon_{AE25})]}} \qquad \text{Eq. 131m- 4}$$

Just as in the ^{133}Xe case, ^{131m}Xe detection efficiency is calculated by the process of creating ratios between the different total decay equations (Eq. 131m-1 through Eq. 131m-4). The first ratio is between the γ-singles and the coincidence (ROI-5).

$$\boldsymbol{\Delta N = \frac{C_{\beta\gamma R5}}{BR_{\gamma 30}\cdot\varepsilon_{\gamma R5}\cdot\varepsilon_{CE129}} = \frac{C_{\gamma R5}}{BR_{\gamma 30}\cdot\varepsilon_{\gamma R5}}} \qquad \text{Eq. 131m- 5}$$

$$\boldsymbol{\frac{C_{\beta\gamma R5}}{C_{\gamma R5}} = \frac{BR_{\gamma 30}\cdot\varepsilon_{\gamma R5}\cdot\varepsilon_{CE129}}{BR_{\gamma 30}\cdot\varepsilon_{\gamma R5}}} \qquad \text{Eq. 131m- 6}$$

After combining terms and simplifying, the resulting detection efficiency for the 129-keV CE is determined.

$$\boldsymbol{\varepsilon_{CE129} = \frac{C_{\beta\gamma R5}}{C_{\gamma R5}}} \qquad \text{Eq. 131m- 7}$$

The next step is to determine the 30-keV X-ray detection efficiency through the ratio of the β-singles to the coincidence. This step is more complicated because the equations leverage almost all of the physics involved; the counts associated with the β-singles needed an extended range to incorporate both the 24.6-keV AE as well as the 160-keV CE (it does not use the defined ROI boundaries). Taking Eq. 131m-1 and Eq. 131m-4, one arrives at Eq. 131m-8.

$$\boldsymbol{\Delta N = \frac{C_{\beta\gamma R5}}{BR_{\gamma 30}\cdot\varepsilon_{\beta\gamma R5}} = \frac{C_\beta}{(BR_{CE160}+BR_{\gamma 30})\cdot\varepsilon_{CE129}+BR_{AE25}\cdot(1-(1-\varepsilon_{CE129})\cdot(1-\varepsilon_{AE25}))}} \qquad \text{Eq. 131m- 8}$$

After recombining terms,

$$\boldsymbol{BR_{\gamma 30}\cdot\varepsilon_{\gamma R5}\cdot\varepsilon_{CE129}\cdot C_\beta = \begin{bmatrix}(BR_{CE160}+BR_{\gamma 30})\cdot\varepsilon_{CE129}+\\ BR_{AE25}\cdot(1-(1-\varepsilon_{CE129})\cdot(1-\varepsilon_{AE25}))\end{bmatrix}\cdot C_{\beta\gamma R5}} \qquad \text{Eq. 131m- 9}$$

Because the 24.6-keV AE has very little impact to the overall detection of ^{131m}Xe (there is only 0.7% difference between 0 % and 100 % efficiency), it is safe to assume it has a similar efficiency to the 129-keV CE. Under this assumption Eq. 131m-9 further simplifies to produce the final equation in determining the X-ray detection efficiency for ^{131m}Xe, Eq. 131m-10.

$$\boldsymbol{\varepsilon_{\gamma R5}} = \frac{\left[\begin{matrix}\left(\boldsymbol{BR_{CE160}}+\boldsymbol{BR_{\gamma 30}}\right)\cdot\boldsymbol{\varepsilon_{CE129}}+ \\ \boldsymbol{BR_{AE25}}\cdot\left(\mathbf{1}-\left(\mathbf{1}-\boldsymbol{\varepsilon_{CE129}}\right)^{\mathbf{2}}\right)\end{matrix}\right]\cdot\boldsymbol{C_{\beta\gamma R5}}}{\boldsymbol{BR_{\gamma 30}}\cdot\boldsymbol{\varepsilon_{CE129}}\cdot\boldsymbol{C_{\beta}}} \qquad \text{Eq. 131m- 10}$$

4.0 Detection Efficiencies for ^{133m}Xe

^{133m}Xe has similar characteristics to ^{131m}Xe; however, unlike ^{131m}Xe, its ground state (^{133}Xe) is unstable (Figures 4.2 and 4.3). Since it decays to ^{133}Xe, there is a continuous source of interference for the ^{133m}Xe efficiency measurement. Removal of the ^{133}Xe from ^{133m}Xe relies on both the ^{133m}Xe (with ^{133}Xe) and pure ^{133}Xe. The subtraction process normalizes the ^{133}Xe spectra (β, γ, and β-γ) using a ratio of the 80-keV γ peak from the ^{133}Xe to the 80-keV γ peak from ^{133}Xe contaminant in the ^{133m}Xe. The normalized ^{133}Xe spectra are then subtracted from the ^{133m}Xe spectra to arrive at nearly pure ^{133m}Xe data.

Once the subtraction is made (and uncertainty propagated), the remaining calculations become nearly identical to those done for ^{131m}Xe. The following calculations are written assuming ^{133m}Xe has been deconvolved from the ^{133}Xe. Initial equations will once again calculate the total number of decays (Eq. 133m-1 through Eq. 133m-4) based on the three signatures: β-singles, γ-singles, and β-γ coincidence.

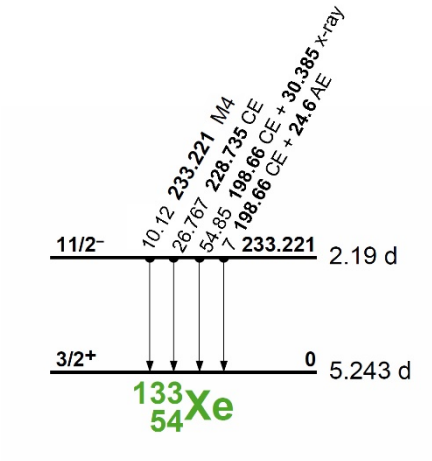

Figure 4.1. Decay Scheme from ^{133m}Xe to ^{133}Xe with Additional Internal Conversion Decay Processes Included

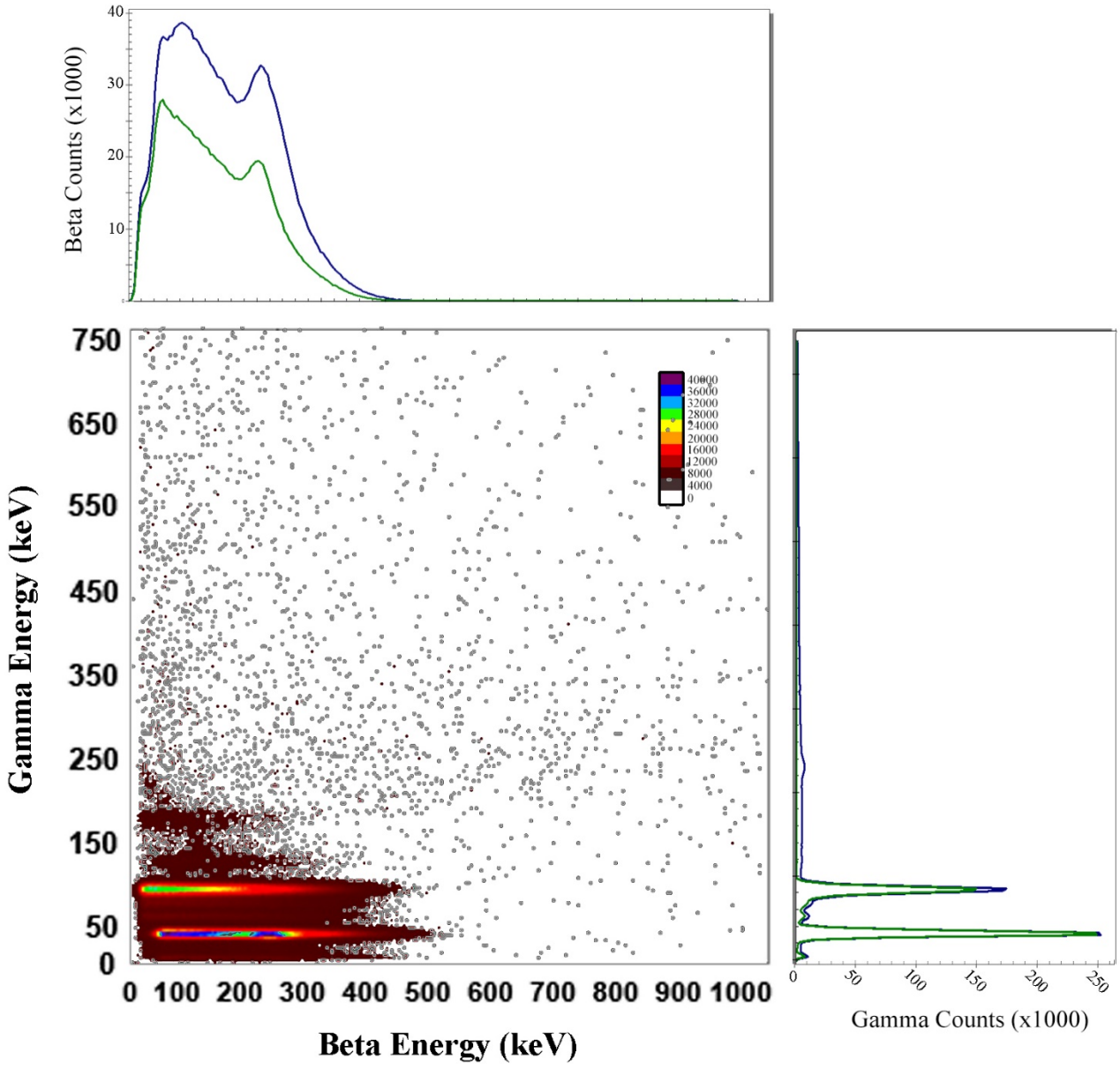

Figure 4.2. Typical ^{133m}Xe Calibration Spectra. The top plot is of β-singles (blue) and the β projection of the β-γ spectrum (green). The right plot is of γ-singles (blue) and the γ projection of the β-γ spectrum (green).

$$\boldsymbol{\Delta N} = \frac{\boldsymbol{C_{\beta\gamma R6}}}{\boldsymbol{BR_{\beta\gamma 30}\cdot\varepsilon_{\beta\gamma R6}}} = \frac{\boldsymbol{C_{\beta\gamma R6}}}{\boldsymbol{BR_{\gamma 30}\cdot\varepsilon_{CE199}\cdot\varepsilon_{\gamma R6}}} \qquad \text{Eq. 133m- 1}$$

$$\boldsymbol{\Delta N} = \frac{\boldsymbol{C_{\gamma R6}}}{\boldsymbol{BR_{\gamma 30}\cdot\varepsilon_{\gamma R6}}} \qquad \text{Eq. 133m- 2}$$

$$\boldsymbol{\Delta N} = \frac{\boldsymbol{C_{\beta}}}{\boldsymbol{BR_{CE229}\cdot\varepsilon_{CE229}+BR_{\gamma 30}\cdot\varepsilon_{CE199}+BR_{AE25}\cdot[1-(1-\varepsilon_{CE199})\cdot(1-\varepsilon_{AE25})]}} \qquad \text{Eq. 133m- 3}$$

The 199-keV CE is in coincidence with the 30-keV X-ray and is therefore relatively easy to calculate. Once the 199-keV CE efficiency is determined, it will be assumed that the 229-keV CE and 24.6-keV AE have similar efficiencies. This assumption is possible for the AE efficiency because it has very little impact on the overall ^{133m}Xe β-γ efficiency. In other words, whether the 24.6-keV AE is 0% or 100%, there is less than a 1% change to the overall ^{133m}Xe detection efficiency. This is can be seen based on the relatively small branching ratio as can be seen below.

$$BR_{\gamma 233} = 10.3\%$$
$$BR_{\beta\gamma} = BR_{\gamma 32} = 56.32\%$$
$$BR_{CE199} = 63.1\%$$
$$BR_{CE229} = 26.86\%$$
$$BR_{AE25} = 6.828\%$$
$$BR_{CE} = BR_{CE199} + BR_{CE229} = 89.96\%$$

The detection efficiency for the 199-keV CE is determined by the ratio of the γ-singles (in this case it is actually X-rays), Eq. 133m-2, and the β-γ coincidence (X-ray coincident with CE), Eq. 133m-1.

$$\boldsymbol{\Delta N = \frac{C_{\beta\gamma R6}}{BR_{\gamma 30}\cdot\varepsilon_{\beta\gamma R6}} = \frac{C_{\gamma R6}}{BR_{\gamma 30}\cdot\varepsilon_{\gamma R6}}} \qquad \text{Eq. 133m- 4}$$

$$\boldsymbol{C_{\gamma R6}\cdot\cancel{BR_{\gamma 30}}\cdot\varepsilon_{\beta\gamma R6} = C_{\beta\gamma R6}\cdot\cancel{BR_{\gamma 30}}\cdot\varepsilon_{\gamma R6}} \qquad \text{Eq. 133m- 5}$$

Since,

$$\boldsymbol{\varepsilon_{\beta\gamma R6} = \varepsilon_{CE199}\cdot\varepsilon_{\gamma R6},}$$

Then,

$$\boldsymbol{C_{\gamma R6}\cdot\varepsilon_{CE199}\cdot\cancel{\varepsilon_{\gamma R6}} = C_{\beta\gamma R6}\cdot\cancel{\varepsilon_{\gamma R6}}} \qquad \text{Eq. 133m- 6}$$

Eq. 133m-6 is solved in terms of ε_{CE199}, arriving at Eq. 133m-7.

$$\boldsymbol{\varepsilon_{CE199} = \frac{C_{\beta\gamma R6}}{C_{\gamma R6}}} \qquad \text{Eq. 133m- 7}$$

Once the 199-keV CE detection efficiency is known, it is time to determine the detection efficiency for the 30-keV X-ray by setting the total number of decays calculated through β-γ coincidence and β-singles equal to each other.

$$\boldsymbol{\Delta N = \frac{C_{\beta\gamma R6}}{BR_{\gamma 30}\cdot\varepsilon_{\beta\gamma R6}} = \frac{C_{\beta}}{\left[\begin{matrix}BR_{CE229}\cdot\varepsilon_{CE229}\\ +BR_{\gamma 30}\cdot\varepsilon_{CE199}\\ +BR_{AE25}\cdot(1-(1-\varepsilon_{CE199})\cdot(1-\varepsilon_{AE25}))\end{matrix}\right]}} \qquad \text{Eq. 133m- 8}$$

Eq. 133m-8 can be simplified by setting, as described earlier, the 229-keV CE and 24.6-keV AE detection efficiencies equal to the 199-keV CE detection efficiency,

$$\boldsymbol{\varepsilon_{CE199} = \varepsilon_{CE229} = \varepsilon_{AE25}.}$$

$$\frac{\boldsymbol{C_{\beta\gamma R6}}}{\boldsymbol{BR_{\gamma 30}\cdot\varepsilon_{\beta\gamma R6}}} = \frac{\boldsymbol{C_{\beta}}}{\begin{bmatrix}\boldsymbol{BR_{CE229}\cdot\varepsilon_{CE199}} \\ \boldsymbol{+BR_{\gamma 30}\cdot\varepsilon_{CE199}} \\ \boldsymbol{+BR_{AE25}\cdot\left(1-(1-\varepsilon_{CE199})\cdot(1-\varepsilon_{CE199})\right)}\end{bmatrix}} \qquad \text{Eq. 133m- 9}$$

After the substitution, Eq. 133m-9, the equation can combine terms to arrive at Eq. 133m-10.

$$\frac{\boldsymbol{C_{\beta\gamma R6}}}{\boldsymbol{BR_{\gamma 30}\cdot\varepsilon_{\beta\gamma R6}}} = \frac{\boldsymbol{C_{\beta}}}{\boldsymbol{(BR_{CE229}+BR_{\gamma 30})\cdot\varepsilon_{CE199}+BR_{AE25}\cdot[1-(1-\varepsilon_{CE199})^2]}} \qquad \text{Eq. 133m- 10}$$

After some additional arranging Eq. 133m-10 becomes Eq. 133m-11.

$$\boldsymbol{BR_{\gamma 30}\cdot\varepsilon_{\beta\gamma R6}\cdot C_{\beta}} = \begin{bmatrix}\boldsymbol{\left(BR_{CE229}+BR_{\gamma 30}\right)\cdot\varepsilon_{CE199}} \\ \boldsymbol{+BR_{AE25}\cdot\left(1-(1-\varepsilon_{CE199})^2\right)}\end{bmatrix}\boldsymbol{\cdot C_{\beta\gamma R6}} \qquad \text{Eq. 133m- 11}$$

Since,

$$\boldsymbol{\varepsilon_{\beta\gamma R6} = \varepsilon_{CE199}\cdot\varepsilon_{\gamma R6}}$$

Then, Eq. 133m-11 becomes Eq. 133m-12

$$\boldsymbol{\varepsilon_{\gamma R6}} = \frac{\begin{bmatrix}\boldsymbol{\left(BR_{CE229}+BR_{\gamma 30}\right)\cdot\varepsilon_{CE199}} \\ \boldsymbol{+BR_{AE25}\cdot\left(1-(1-\varepsilon_{CE199})^2\right)}\end{bmatrix}\boldsymbol{\cdot C_{\beta\gamma R6}}}{\boldsymbol{\varepsilon_{CE199}\cdot BR_{\gamma 30}\cdot C_{\beta}}} \qquad \text{Eq. 133m- 12}$$

5.0 Detection Efficiencies for ^{135}Xe

The final xenon isotope used in the efficiency calibration is ^{135}Xe. It is usually the first isotope measured in the calibration procedure because of its short half-life. The detection efficiency of ^{135}Xe is one of the easiest to calculate because it has one dominate decay that has a 249.77-keV γ-ray in coincidence with the β decay (Figures 5.1 and 5.2).

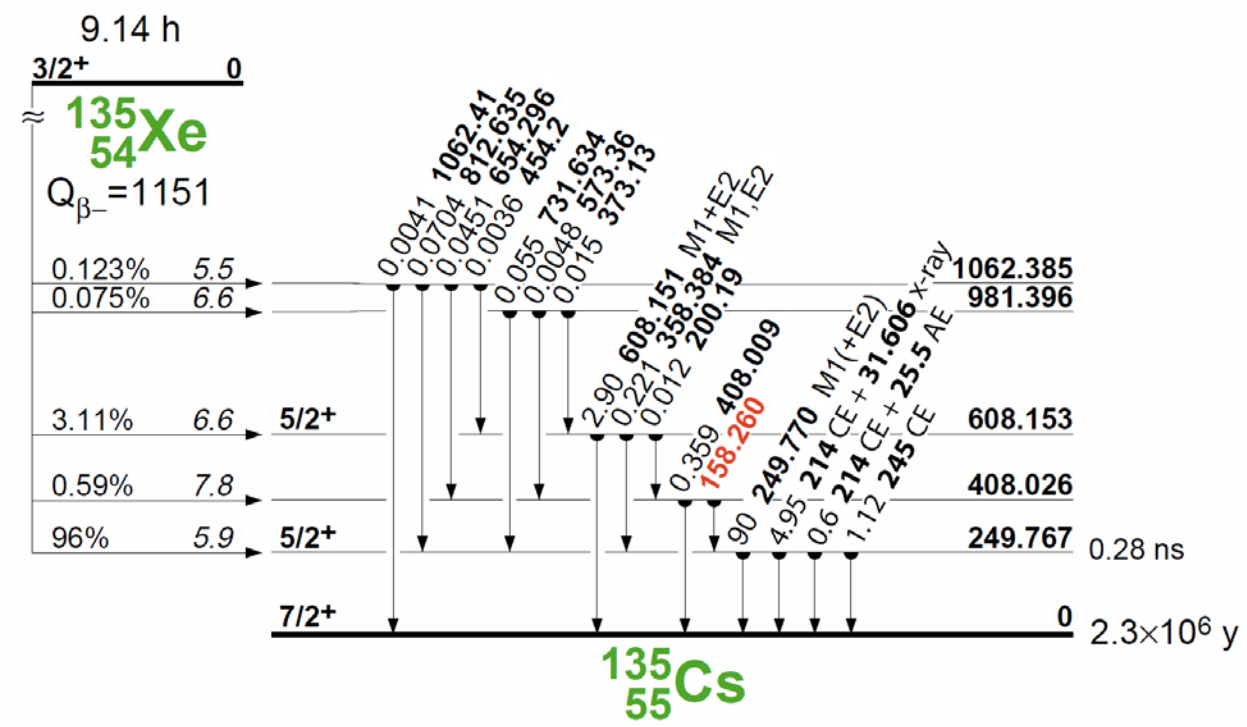

Figure 5.1. Decay Scheme from ^{135}Xe to ^{135}Cs with Additional Internal Conversion Decay Processes Included

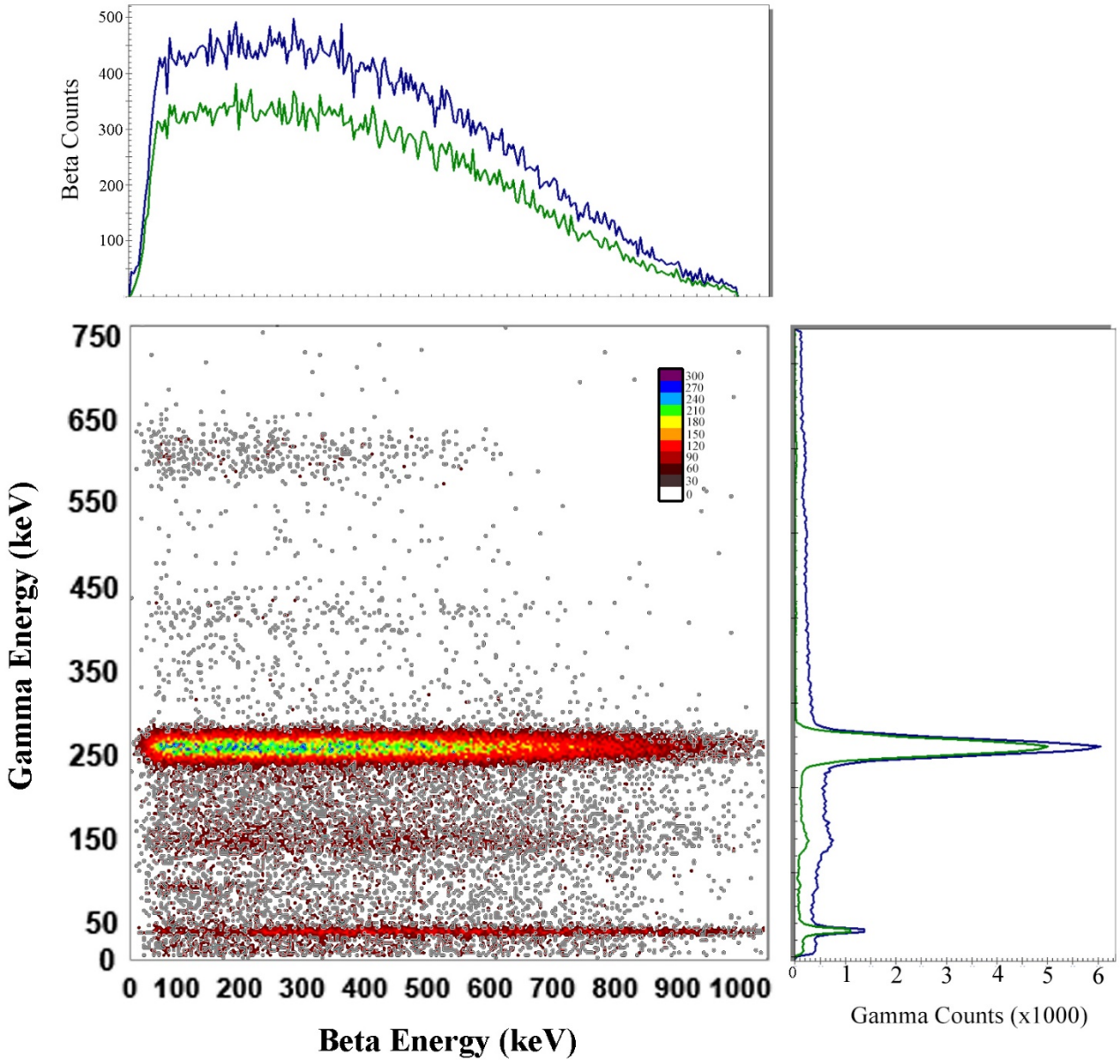

Figure 5.2. Typical ^{135}Xe Calibration Spectra. The top plot is of β-singles (blue) and the β projection of the β-γ spectrum (green). The right plot is of γ-singles (blue) and the γ projection of the β-γ spectrum (green).

For the purposes of the efficiency calibration all three signatures: γ-singles, β-singles, and β-γ coincidence are used (Eq. 135-1 through Eq. 135-5).

$$\boldsymbol{\Delta N} = \frac{\boldsymbol{C_{\beta\gamma R2}}}{\boldsymbol{BR_{\beta\gamma 250}\cdot\varepsilon_{\beta\gamma R2}}} = \frac{\boldsymbol{C_{\beta\gamma R2}}}{\boldsymbol{BR_{\gamma 250}\cdot\varepsilon_{\beta}\cdot\varepsilon_{\gamma R2}}} \qquad \text{Eq. 135- 1}$$

$$\boldsymbol{\Delta N = \frac{C_{\gamma R2}}{BR_{\gamma 250}\cdot\varepsilon_{\gamma R2}}} \qquad \text{Eq. 135- 2}$$

$$\boldsymbol{\Delta N = \frac{C_{\beta}}{BR_{\gamma 250}\cdot\varepsilon_{\beta}+\begin{bmatrix} BR_{CE245}\cdot[1-(1-\varepsilon_{\beta})\cdot(1-\varepsilon_{CE245})] \\ +BR_{\gamma 32}\cdot[1-(1-\varepsilon_{\beta})\cdot(1-\varepsilon_{CE214})] \\ +BR_{AE26}\cdot[1-(1-\varepsilon_{\beta})\cdot(1-\varepsilon_{CE214})\cdot(1-\varepsilon_{AE26})]\end{bmatrix}}} \qquad \text{Eq. 135- 3}$$

$$\boldsymbol{\Delta N = \frac{C_{\beta\gamma 32}}{\varepsilon_{\gamma 32}\cdot BR_{\gamma 32}\cdot[1-(1-\varepsilon_{\beta})\cdot(1-\varepsilon_{CE214})]}} \qquad \text{Eq. 135- 4}$$

$$\boldsymbol{\Delta N = \frac{C_{\gamma 32}}{BR_{\gamma 32}\cdot\varepsilon_{\gamma 32}}} \qquad \text{Eq. 135- 5}$$

Because the AE has a 0.6% branching ratio (see the branching ratios given below), it provides an insignificant contribution to the overarching ^{135}Xe detection efficiency. Therefore, the detection efficiency for the 25.5-keV AE will be assumed to be the same as for the 214-keV and 245-keV CE.

$$BR_{\beta\gamma 250} \cong BR_{\gamma 250} = 90.0\%$$
$$BR_{\gamma 32} = 4.95\%$$
$$BR_{AE26} = 0.6\%$$
$$BR_{CE245} = 1.12\%$$

Because the 250-keV is coincidence with only a β, it provides and easy mechanism to determine the β efficiency for ^{135}Xe. By setting Eq. 135-1 and Eq. 135-2 equal, one is able to determine the β efficiency.

$$\boldsymbol{\Delta N = \frac{C_{\beta\gamma R2}}{BR_{\gamma 250}\cdot\varepsilon_{\beta\gamma R2}} = \frac{C_{\gamma R2}}{BR_{\gamma 250}\cdot\varepsilon_{\gamma R2}}} \qquad \text{Eq. 135- 6}$$

After solving Eq. 135-6 for $\boldsymbol{\varepsilon_{\beta\gamma R2}}$, one arrives at Eq. 135-7.

$$\boldsymbol{\varepsilon_{\beta\gamma R2} = \frac{C_{\beta\gamma R2}\cdot BR_{\gamma 250}\cdot\varepsilon_{\gamma R2}}{C_{\gamma R2}\cdot BR_{\gamma 250}}} \qquad \text{Eq. 135- 7}$$

By substituting $\varepsilon_{\beta\gamma 250} = \varepsilon_{\beta}\cdot\varepsilon_{\gamma 250}$ and canceling terms one gets Eq. 135-8 and Eq. 135-9.

$$\boldsymbol{\varepsilon_{\beta}\cdot\cancel{\varepsilon_{\gamma R2}} = \frac{C_{\beta\gamma R2}\cdot\cancel{BR_{\gamma 250}}\cdot\cancel{\varepsilon_{\gamma R2}}}{C_{\gamma R2}\cdot\cancel{BR_{\gamma 250}}}} \qquad \text{Eq. 135- 8}$$

$$\boldsymbol{\varepsilon_{\beta} = \frac{C_{\beta\gamma R2}}{C_{\gamma R2}}} \qquad \text{Eq. 135- 9}$$

Now that the β efficiency has been determined, the next step is to determine the detection efficiency for the 214-keV CE by setting the 32-keV β-γ and γ-singles total decay equations (Eq. 135-4 and Eq. 135-5) equal.

$$\boldsymbol{\Delta N = \frac{C_{\beta\gamma 32}}{\varepsilon_{\gamma 32}\cdot BR_{\gamma 32}\cdot[1-(1-\varepsilon_{\beta})\cdot(1-\varepsilon_{CE214})]} = \frac{C_{\gamma 32}}{BR_{\gamma 32}\cdot\varepsilon_{\gamma 32}}} \qquad \text{Eq. 135- 10}$$

Eq. 135-10 simplifies through cancelation of terms.

$$\frac{C_{\beta\gamma 32}}{\varepsilon_{\gamma 32}\cdot BR_{\gamma 32}\cdot\left[1-(1-\varepsilon_\beta)\cdot(1-\varepsilon_{CE214})\right]}=\frac{C_{\gamma 32}}{BR_{\gamma 32}\cdot\varepsilon_{\gamma 32}}. \qquad \text{Eq. 135- 11}$$

Then, Eq. 135-11 can be rewritten as Eq. 135-12.

$$\frac{C_{\beta\gamma 32}}{C_{\gamma 32}}=1-\left(1-\varepsilon_\beta\right)\cdot\left(1-\varepsilon_{CE214}\right) \qquad \text{Eq. 135- 12}$$

After solving Eq. 135-12 one arrives at Eq. 135-13, which will be used to simplify the β-singles equations for the remaining calculations.

$$\varepsilon_{CE214}=1-\frac{\left(1-\frac{C_{\beta\gamma 32}}{C_{\gamma 32}}\right)}{(1-\varepsilon_\beta)} \qquad \text{Eq. 135- 13}$$

The next step is to determine the 250-keV γ efficiency by setting Eq. 135-1 equal to Eq. 135-3.

$$\Delta N=\frac{C_{\beta\gamma R2}}{BR_{\gamma 250}\cdot\varepsilon_{\beta\gamma R2}}$$

$$=\frac{C_\beta}{BR_{\gamma 250}\cdot\varepsilon_\beta+\begin{bmatrix}BR_{CE245}\cdot\left[1-(1-\varepsilon_\beta)\cdot(1-\varepsilon_{CE245})\right]\\+BR_{\gamma 32}\cdot\left[1-(1-\varepsilon_\beta)\cdot(1-\varepsilon_{CE214})\right]\\+BR_{AE26}\cdot\left[1-(1-\varepsilon_\beta)\cdot(1-\varepsilon_{CE214})\cdot(1-\varepsilon_{AE26})\right]\end{bmatrix}} \qquad \text{Eq. 135- 14}$$

Which in turn simplifies Eq. 135-14.

$$BR_{\gamma 250}\cdot\varepsilon_{\beta\gamma \mathrm{R2}}\cdot C_\beta=\begin{bmatrix}BR_{\gamma 250}\cdot\varepsilon_\beta\\+BR_{CE245}\cdot\left[1-\left(1-\varepsilon_\beta\right)\cdot\left(1-\varepsilon_{CE214}\right)\right]\\+BR_{\gamma 32}\cdot\left[1-\left(1-\varepsilon_\beta\right)\cdot\left(1-\varepsilon_{CE214}\right)\right]\\+BR_{AE26}\cdot\left[1-\left(1-\varepsilon_\beta\right)\cdot\left(1-\varepsilon_{CE214}\right)^2\right]\end{bmatrix}\cdot C_{\beta\gamma \mathrm{R2}} \qquad \text{Eq. 135- 15}$$

After combining terms and recalling that $\varepsilon_{\beta\gamma 250}=\varepsilon_\beta\cdot\varepsilon_{\gamma \mathrm{R2}}$ Eq. 135-15 becomes Eq. 135-16, the final 250-keV γ efficiency equation.

$$\varepsilon_{\gamma \mathrm{R2}}=\frac{\begin{bmatrix}BR_{\gamma 250}\cdot\varepsilon_\beta\\+\left(BR_{CE245}+BR_{\gamma 32}\right)\cdot\left[1-\left(1-\varepsilon_\beta\right)\cdot\left(1-\varepsilon_{CE214}\right)\right]\\+BR_{AE26}\cdot\left[1-\left(1-\varepsilon_\beta\right)\cdot\left(1-\varepsilon_{CE214}\right)^2\right]\end{bmatrix}\cdot C_{\beta\gamma \mathrm{R2}}}{\varepsilon_\beta\cdot BR_{\gamma 250}\cdot C_\beta} \qquad \text{Eq. 135- 16}$$

6.0 Energy Resolution

The full width at half maximum (FWHM) of the peaks found in Table 1.2 must also be determined to create a relationship between the detector energy and the resolution. The FWHM and uncertainty in units keV of at least two points in the β energy must be found and six points in the γ energy. To determine the resolutions, a Gaussian must be fitted to each peak where

$$f(E) = ae^{-(E-\mu b)^2/2\sigma c^2}\ , \qquad \text{Eq. 6–1}$$

where α is the amplitude of the peak, μ is the centroid of the peak, and σ is the variance. The FWHM is related to the variance of the Gaussian by

$$FWHM = 2\sqrt{2ln2}\sigma \approx 2.35482\sigma. \qquad \text{Eq. 6–2}$$

The two β points are determined from ^{131m}Xe and ^{133m}Xe conversion electrons. It is not recommended to use the 45-keV CE from ^{133}Xe as there may be clipping on the lower end of the peak due to detector threshold limits that will affect the FWHM calculations. Fitting the ^{131m}Xe CE β peak at 129.4 keV should be done using only the projection of the ROI 5 onto the β axis. This will reduce any broadening of the Gaussian peak due to Compton scattering and ensure a more accurate FWHM calculation. Additionally, the β-singles spectrum of ^{131m}Xe also contains several other peaks around 160 keV. Although these CEs are coincident with x-rays, the x-rays are at low energies of 3.7 keV and 5.3 keV ($\bar{E} \approx 4.5$ keV) and are not present in the coincident spectrum. The additional peaks broaden the β-singles spectrum as seen in Figure 3.2. Higher resolution β detectors such as silicon should be able to differentiate these peaks, but plastic scintillators will not.

Determine the FWHM of the ^{133m}Xe CE at 198.6 keV requires a little more attention due to the presence of ^{133}Xe in the sample. Similar to ^{131m}Xe, the coincidence spectrum must be used for the fit to eliminate the higher energy CEs that are present from ^{133m}Xe. The β-singles spectrum contains peaks from the 227.8 keV L-shell CE and 232 M-shell CE. Deconvolution of the ^{133m}Xe peak from the ^{133}Xe spectrum requires the use of the isotopically pure ^{133}Xe spectrum. The projection of the 30-keV ^{133}Xe spectrum (ROI 4) can be normalized to the ^{133m}Xe spectrum by looking at a ratio of counts in the 80-keV region. The β spectrum from the ^{133}Xe can then be subtracted to reveal the ^{133m}Xe CE spectrum. A Gaussian can then be fitted to this peak to determine the FWHM.

Determining the FWHM of γ-ray peaks is straightforward. Use of the coincidence spectrum reduces the background spectrum but is typically unnecessary due to the shortened length of the calibration count. The measurement of all radionuclides are required to complete the energy resolution measurement. The 661.7 keV energy peak from ^{137}Cs is not be used as a measurement for resolution as it does not accurately represent γ emitted from a source in the β-cell.

7.0 Conclusion

The absolute calibration method, although generally known, is new in the application to radioxenon β-γ detectors. Previous calibration techniques rely upon known standards that are often difficult to use because of the levels of activity and constraints on what isotopes are available. The absolute method removes some of these difficulties by no longer requiring standards. Instead, the method relies on the isotopic purity of the samples (efforts are ongoing to remove purity as a constraint).

The method leverages the three combinations of data generated by a β-γ detector: γ-singles, β-singles, and β-γ coincidence. By intelligently analyzing the data sets, one is able to take advantage of the most significant physics contributions to make a model that results in the determination of the total number of decays in a given measurement. Given the total number of decays, determining the detection efficiency for each decay path is a relatively process. The advantage of this method is that it allows accurate efficiency calculations without knowing the sample activity in advance while reducing the sources of uncertainty.

8.0 References

Arthur R, T Bowyer, J Hayes, T Heimbigner, J McIntyre, H Miley, and M Panisko. 2001. "Radionuclide Measurements for Nuclear Explosion Monitoring." In *Proceedings of the 23rd Seismic Research Review: Worldwide Monitoring of Nuclear Explosions, October 2-5, 2001, Jackson Hole, Wyoming, Volume II*, LA-UR-01-4454, National Nuclear Security Administration and the Defense Threat Reduction Agency, Washington, DC.

Auer M, T Kumberg, H Sartorius, B Wernsperger, and C Schlosser. 2010. "Ten Years of Development of Equipment for Measurement of Atmospheric Radioactive Xenon for the Verification of the CTBT." *Pure and Applied Geophysics*, 167(4-5):471-486.

Bowyer TW, KH Abel, CW Hubbard, AD McKinnon, ME Panisko, RW Perkins, PL Reeder, RC Thompson, and RA Warner. 1998. "Automated Separation and Measurement of Radioxenon for the Comprehensive Test Ban Treaty." *Journal of Radioanalytical and Nuclear Chemistry*, 235(1-2):77-82.

Bowyer TW, JI McIntyre, and PL Reeder. 1999. "High Sensitivity Detection of Xe Isotopes Via β-γ Coincidence Counting." In *Proceedings of the 21st Seismic Research Symposium: Technologies for Monitoring Comprehensive Nuclear-Test-Ban Treaty, Las Vegas, NV, Sep. 21-24, 1999*. LA-UR-99-4700.

Bowyer, TW, JC Hayes, PL Reeder, ME Panisko, WK Pitts, JI McIntyre, KH Abel, RC Thompson, TR Heimbigner, RA Warner. 2000. "Automated Radioxenon Sampler-Analyzer: Detection of Radioactive Xenon for the CTBT." In *Abstracts of Papers of the American Chemical Society*. American Chemical Society, Washington, DC.

Bowyer TW**,** PE Dresel, JC Hayes, JI McIntyre, HS Miley, and KB Olsen. 2006. "Environmental Applications for Radioactive Xenon Monitoring." Abstract submitted to 10th Environmental Radiochemical Analysis Symposium, Oxford, United Kingdom. PNNL-SA-49459. Published in *10TH INTERNATIONAL SYMPOSIUM ON Environmental Radiochemical Analysis*. Royal Society of Chemistry, The Randolph Hotel, Oxford, UK.

Bowyer T, M Cooper, JC Hayes, J Forrester, D Haas, R Hansen, P Keller, R Kirkham, L Lidey, JI McIntyre, HS Miley, P Payne, P Saey, RC Thompson, R Williams, and V Woods. 2009. *Measurements of Worldwide Radioxenon Backgrounds–The "EU" Project*. PNNL-18783, Pacific Northwest National Laboratory, Richland, Washington.

Bowyer TW, SR Biegalski, M Cooper, D Haas, JC Hayes, HS Miley, DJ Strom, and V Woods. 2011. "Elevated Radioxenon Detected Remotely Following the Fukushima Nuclear Accident." *Journal of Environmental Radioactivity*, 102(7):681-687.

Carman AJ, JI McIntyre, JC Hayes, DE Coomes, TR Heimbigner, KE Litke, SJ Morris, MD Ripplinger, and R Suarez. 2005. "Characterization of the γ Detection of CsI(Tl), CsI(Na), and NaI(Tl) Well Detectors." PNNL-SA-44711, Pacific Northwest National Laboratory, Richland, Washington.

Cooper, MW, AJ Carman, JC Hayes, TR Heimbigner, CW Hubbard, KE Litke, JI McIntyre, SJ Morris, MD Ripplinger, and R Suarez. 2005. “Improved β-γ Coincidence Detector for Radioxenon Detection.” In *Proceedings of the 27th Seismic Research Review: Ground-Based Nuclear Explosion Monitoring Technologies*, LA-UR-05-6407. National Nuclear Security Administration and Air Force Research Association, Washington, DC. pp. 779-786.

Cooper MW, TW Bowyer, JC Hayes, JI McIntyre, MD Ripplinger, R Suarez, TR Heimbigner, BT Schrom, CW Hubbard. 2007a. “β-γ Detection System Improvements and Calibration.” International Noble Gas Experiment, Las Vegas, Nevada, November 5, 2007, PNNL-SA-57904.

Cooper, MW, JI McIntyre, TW Bowyer, AJ Carman, JC Hayes, TR Heimbigner, CW Hubbard, L Lidey, KE Litke, SJ Morris, MD Ripplinger, R Suarez, and R Thompson. 2007b. “Redesigned β-γ Radioxenon Detector.” *Nuclear Instruments & Methods in Physics Research Section a-Accelerators Spectrometers Detectors and Associated Equipment*, 579(1):426-430.

Cooper MW, TW Bowyer, JC Hayes, JI McIntyre, MD Ripplinger, R Suarez, TR Heimbigner, BT Schrom, CW Hubbard. 2013a. “Absolute Efficiency Calibration of a β-γ Detector.” *IEEE Transactions on Nuclear Science*, 60(2):676-680.

Cooper MW, JH Ely, JI McIntyre, BT Schrom, and TJ Suckow. 2013. "Standalone Calibration Tool." 2014 AGU Fall Meeting, San Francisco, CA on December 10, 2013. PNNL-SA-99885.

Ely JH**,** MW Cooper, DA Haas, JC Hayes, JI McIntyre, and BT Schrom. 2010. "Automating Calibration Analysis for Beta-Gamma Detectors." International Noble Gas Experiment, Buenos Aires, Argentina on November 1, 2010. PNNL-SA-75960.

Gohla H, M Auer, Ph Cassette, RK Hague, M Lechermann, and B Nadalut. 2016. “Radioxenon standards Used in Laboratory Inter-Comparisons.” *Applied Radiation and Isotopes*, 109:24-29.

Haas DA, SR Biegalski, and KM Folz Biegalski. 2009. “Radioxenon Production Through Neutron Irradiation of Stable Xenon Gas.” *Journal of Radioanalytical and Nuclear Chemistry*, 282(3):677-680.

Hayes JC, KH Abel, TW Bowyer, TR Heimbigner, ME Panisko, PL Reeder, JI McIntyre, RC Thompson, LC Todd, and RA Warner. 1999. “Operations of the Automated Radioxenon Sampler/Analyzer—ARSA.” *Proceedings of the 21st Seismic Research Symposium: Technologies for Monitoring the Comprehensive Nuclear-Test-Ban Treaty*, p. 249-260.

Hennig W, H Tan, A Fallu-Labruyere, WK Warburton, JI McIntyre, and A Gleyzer. 2006a. "Design of a Phoswich Well Detector for Radioxenon Monitoring." In *28th Seismic Research Review - Ground Based Nuclear Explosion Monitoring Technologies*, Orlando, FL, Sept. 19-21, 2006, pp. 801-810

Hennig W, H Tan, WK Warburton, and JI McIntyre. 2006b. “Scintillation Detectors-Single-Channel β-γ Coincidence Detection of Radioactive Xenon Using Digital Pulse Shape Analysis of Phoswich Detector Signals.” *IEEE Transactions on Nuclear Science*, 53(2):620-624.

Hennig, Wolfgang, Tan, Hui, Fallu-Labruyere, A., Warburton, William K., McIntyre, Justin I., and Gleyzer, A. “A Phoswich Well Detector for Radioxenon Monitoring.” *Nuclear Instruments and Methods*

in Physics Research A: Accelerators, Spectrometers, Detectors and Associated Equipment, Volume 579, Issue 1, 2007, p. 431-436, https://doi.org/10.1016/j.nima.2007.04.093.

Houghton T, CA McGrath, RK Hague, JG Eisenmenger, and TA Robinson. 2016. "Isolation and Purification of the Xenon fraction of ^{252}Cf Spontaneous Fission Products for the Production of Radioactive Xenon Calibration Standards." *Journal of Radioanalytical and Nuclear Chemistry*, 307(3):2557-2562.

Knoll, GF. 2010. *Radiation Detection and Measurement*. John Wiley & Sons, Hoboken, New Jersey.

Le Petit G, C Jutier, P Gross, and V Greiner. 2006. "Low-level Activity Measurement of ^{131}Xe^{m}, ^{133}Xe^{m}, ^{135}Xe, and ^{133}Xe in Atmospheric Air Samples Using High-Resolution Dual X-γ Spectrometry." *Applied Radiation and Isotopes*, 64(10-11):1307-1312.

Le Petit G, P Armand, G Brachet, T Taffary, JP Fontaine, P Achim, X Blanchard, JC Piwowarczyk, and F Pointurier. 2008. "Contribution to the Development of Atmospheric Radioxenon Monitoring." *Journal of Radioanalytical and Nuclear Chemistry*, 276(2):391-398.

McGrath CA, TP Houghton, JK Pfeiffer, and RK Hague. 2013. "Xe-135 Production from Cf-252." *Journal of Radioanalytical and Nuclear Chemistry*, 296(2):893-897.

McIntyre JI, KH Abel, TW Bowyer, JC Hayes, TR Heimbigner, ME Panisko, PL Reeder, and RC Thompson. 2001. "Measurements of Ambient Radioxenon Levels Using the Automated Radioxenon Sampler/Analyzer (ARSA)." *Journal of Radioanalytical and Nuclear Chemistry*, 248(3):629-635.

McIntyre JI, TW Bowyer, MW Cooper, and JC Hayes. 2007. "Triple Coincidence Detection Techniques." International Noble Gas Experiment, Las Vegas, NV on November 5, 2007. PNNL-SA-57913.

McIntyre JI, SL Pratt, TW Bowyer, MW Cooper, JC Hayes, TR Heimbigner, CW Hubbard, HS Miley, and MD Ripplinger. 2008. "Generation of Radioxenon Isotopes." Chapter 5 in *Proceedings of the 30th Monitoring Research Review: Ground-Based Nuclear Explosion Monitoring Technologies*, pp. 793-801. Los Alamos National Laboratory, Los Alamos, NM.

McIntyre JI, BT Schrom, JH Ely, MW Cooper, DA Haas. 2012. "Stand-Alone Calibration Tool." International Noble Gas Experiment, Mito City, Ibaraki, Japan on November 5, 2012. PNNL-SA-91604.

NCRP - National Council on Radiation Protection and Measurements. 1985. *A Handbook of Radioactivity Measurements Procedures.* Report 058. NCRP, Bethesda, Maryland.

Prelovskii VV, NM Kazarinov, A Yu Donets, V Yu Popov, I Yu Popov, and NV Skirda. 2007. "The ARIX-03F mobile semiautomatic facility for measuring low concentrations of Radioactive Xenon Isotopes in Air and Subsoil Gas." *Instruments and Experimental Techniques*, 50(3):393-397.

Reeder PL, TW Bowyer, JI McIntyre, WK Pitts, A Ringbom, and C Johansson. 2004. "Gain Calibration of a β/γ Coincidence Spectrometer for Automated Radioxenon Analysis." *Nuclear Instruments and Methods in Physics Research Section A: Accelerators, Spectrometers, Detectors*, 521(2):586-599.

Ringbom A, T Laron, A Axelsson, K Elmgren, and C Johansson. 2003. “SAUNA - a System for Automatic Sampling, Processing, and Analysis of Radioactive Xenon.” *Nuclear Instruments and Methods in Physics Research Section A*, 508(3):542-553.

Ringbom, A. 2005. “Verifying the Comprehensive Nuclear-Test-Ban Treaty by Radioxenon Monitoring.” In *International Conference on Nuclear Data for Science and Technology, Pts 1 and 2*, pp. 1693-1697.

Saey PRJ. 2009. “The Influence of Radiopharmaceutical Isotope Production on the Global Radioxenon Background.” *Journal of Environmental Radioactivity*, 100(5):396-406.

Saey PRJ, A Ringbom, TW Bowyer, M Zähringer, M Auer, A Faanhof, C Labuschagne, MS Al-Rashidi, U Tippawan, and B Verboomen. 2013. “Worldwide Measurements of Radioxenon Background Near Isotope Production Facilities, a Nuclear Power Plant and at Remote Sites: the ‘EU/JA-II’ Project.” *Journal of Radioanalytical and Nuclear Chemistry*, 296(2):1133-1142.

Watrous MG, JE Delmore, RK Hague, TP Houghton, DD Jenson, and NR Mann. 2015. “Radioxenon Spiked Air.” *Journal of Environmental Radioactivity*, 150:126-131.

Pacific Northwest
NATIONAL LABORATORY

U.S. DEPARTMENT OF
ENERGY

Proudly Operated by **Battelle** *Since 1965*

902 Battelle Boulevard
P.O. Box 999
Richland, WA 99352
1-888-375-PNNL (7665)

www.pnnl.gov